Available online at www.sciencedirect.com

ScienceDirect

Geochimica et Cosmochimica Acta 180 (2016) 146–163

Geochimica et Cosmochimica Acta

www.elsevier.com/locate/gca

Open system sulphate reduction in a diagenetic environment – Isotopic analysis of barite ($\delta^{34}S$ and $\delta^{18}O$) and pyrite ($\delta^{34}S$) from the Tom and Jason Late Devonian Zn–Pb–Ba deposits, Selwyn Basin, Canada

J.M. Magnall [a,*,1], S.A. Gleeson [a,1], R.A. Stern [a], R.J. Newton [b], S.W. Poulton [b], S. Paradis [c]

[a] Department of Earth and Atmospheric Sciences, University of Alberta, Edmonton, Alberta T6G 2E3, Canada
[b] School of Earth and Environment, University of Leeds, Leeds LS2 9JT, UK
[c] Geological Survey of Canada, Box 6000, 9860 West Saanich Road, Sidney, British Columbia V8L 4B2, Canada

Received 4 March 2015; accepted in revised form 10 February 2016; available online 16 February 2016

Abstract

Highly positive $\delta^{34}S$ values in sulphide minerals are a common feature of shale hosted massive sulphide deposits (SHMS). Often this is attributed to near quantitative consumption of seawater sulphate, and for Paleozoic strata of the Selwyn Basin (Canada), this is thought to occur during bacterial sulphate reduction (BSR) in a restricted, euxinic water column. In this study, we focus on drill-core samples of sulphide and barite mineralisation from two Late Devonian SHMS deposits (Tom and Jason, Macmillan Pass, Selwyn Basin), to evaluate this euxinic basin model. The paragenetic relationship between barite, pyrite and hydrothermal base metal sulphides has been determined using transmitted and reflected light microscopy, and backscatter electron imaging. This petrographic framework provides the context for in-situ isotopic microanalysis (secondary ion mass spectrometry; SIMS) of barite and pyrite. These data are supplemented by analyses of $\delta^{34}S$ values for bulk rock pyrite ($n = 37$) from drill-core samples of un-mineralised (barren), siliceous mudstone, to provide a means by which to evaluate the mass balance of sulphur in the host rock.

Three generations of barite have been identified, all of which pre-date hydrothermal input. Isotopically, the three generations of barite have overlapping distributions of $\delta^{34}S$ and $\delta^{18}O$ values (+22.5‰ to +33.0‰ and +16.4‰ to +18.3‰, respectively) and are consistent with an origin from modified Late Devonian seawater. Radiolarian tests, enriched in barium, are abundant within the siliceous mudstones, providing evidence that primary barium enrichment was associated with biologic activity. We therefore propose that barite formed following remobilisation of productivity-derived barium within the sediment, and precipitated within diagenetic pore fluids close to the sediment water interface. Two generations of pyrite are texturally associated with barite: framboidal pyrite (py-I), which has negative $\delta^{34}S$ values (−23‰ to −28‰; $n = 9$), and euhedral pyrite (py-II), which has markedly more positive $\delta^{34}S$ values (+8‰ to +26‰; $n = 86$). We argue that stratiform pyrite and barite developed along diagenetic redox fronts, where the isotopic relationships ($\delta^{34}S_{pyrite} \approx \delta^{34}S_{barite}$) are explained by anaerobic oxidation of methane coupled to sulphate reduction (AOM-SR). Furthermore, the relatively narrow distribution of $\delta^{34}S_{barite}$ values is consistent with an open system model of sulphate reduction, in which reduced sulphur generation occurred with a reduced isotopic fractionation ($\varepsilon^{34}S = <15‰$) linked to higher rates of sulphate reduction and AOM-SR. Importantly, hydrothermal sulphides (pyrite, sphalerite and galena) all post-date this diagenetic barite-pyrite assemblage, and textural and

* Corresponding author.
E-mail addresses: magnall@gfz-potsdam.de, joseph.magnall@gmail.com (J.M. Magnall).
[1] Current address: Helmholtz Centre Potsdam, GFZ German Research Centre for Geosciences, 14473 Potsdam, Germany.

http://dx.doi.org/10.1016/j.gca.2016.02.015
0016-7037/

mineralogical evidence indicates barite replacement to be an important process during hydrothermal mineralisation. Neither the textures nor the documented isotopic relationships can be produced by processes operating in a euxinic water column, which represents a major departure from the conventional model for SHMS formation at Macmillan Pass. We suggest that positive $\delta^{34}S$ values in sulphides, a common feature of SHMS systems both in the Selwyn Basin and throughout the geologic record, could be linked to AOM-SR. At Macmillan Pass, positive $\delta^{34}S_{pyrite}$ values developed during open system diagenesis, which was critical for rapid sulphur cycling and the development of an effective metal trap.

1. INTRODUCTION

The distribution of shale-hosted massive sulphide (SHMS) deposits (Leach et al., 2005, 2010) in the geological record has led to the suggestion that secular changes in ocean chemistry impart a fundamental control on ore genesis (Goodfellow and Jonasson, 1984; Turner, 1992; Lyons et al., 2006; Farquhar et al., 2010). In essence, these deposits represent anomalous accumulations of reduced sulphur in marine strata, the origin of which is widely accepted to be seawater sulphate (Ohmoto and Goldhaber, 1997). Thus, sulphate availability and the mechanism of sulphate reduction are both key factors in models of metallogenesis.

In marine strata, bacterial sulphate reduction (BSR) is the most important geochemical pathway for sulphide production; typically, this occurs in the diagenetic environment beneath the sediment water interface (SWI) where chemical, physical and biological processes produce organic and inorganic transformations in recently deposited sediments (for reviews of diagenesis, see Berner, 1980; Emerson and Hedges, 2003; Aller, 2014). A large kinetic isotope fractionation is associated with BSR, due to the preferential selection, by bacteria, of sulphate molecules containing ^{32}S and ^{16}O (Kaplan and Rittenberg, 1964; Mizutani and Rafter, 1973). This can be expressed in standard delta (δ) notation in units of ‰, where $\delta = [(R_{sample} - R_{standard})/(R)_{standard}] \times 10^3$, and R is either $^{34}S/^{32}S$ or $^{18}O/^{16}O$ in the sample or standard.

Negative $\delta^{34}S$ values are characteristic of sedimentary pyrite formed in the Paleozoic, which is the dominant sink for sulphide produced via BSR (Canfield, 2004). However, it is also possible to produce a broad range of $\delta^{34}S$ values during BSR, and the magnitude of the sulphur isotope fractionation ($\varepsilon^{34}S = \delta^{34}S_{SO4} - \delta^{34}S_{H2S}$) is dependent on a number of factors, including: sulphate reduction rate (Kaplan and Rittenberg, 1964), substrate type (Canfield, 2001a), sulphate concentration (Habicht et al., 2002), and reaction reversibility of intracellular steps (Rees, 1973; Brunner and Bernasconi, 2005; Bradley et al., 2011). Furthermore, the $\delta^{34}S$ values that are preserved by sulphate and sulphide minerals may be influenced by transport limitation governed by sedimentological factors (Goldhaber and Kaplan, 1975; Aller et al., 2010) and the effects of differential isotopic diffusion (Jørgensen et al., 2004). In the geologic record, which often lacks spatially (and temporally) resolved constraints for coeval $\delta^{34}S$ values in sulphate and sulphide, the interpretation of isotopic data can therefore be challenging (see recent discussion in Fike et al., 2015). Indeed, commonly it is simply the difference between constraints for seawater sulphate (e.g. carbonate associated sulphate, CAS; Bottrell and Newton, 2006) and $\delta^{34}S_{pyrite}$ values that are discussed ($\Delta^{34}S_{CAS\text{-}Py} = \delta^{34}S_{CAS} - \delta^{34}S_{pyrite}$), which often represents sulphur derived from different environments (Gomes and Hurtgen, 2015).

A characteristic feature of sulphides in SHMS deposits are positive $\delta^{34}S$ values (Lyons et al., 2006), which, when encountered in marine sediments from un-mineralised settings, are thought to represent periods of severe sulphate limitation. Such conditions may develop on a variety of scales, from within the cell membranes of sulphate reducing microorganisms (Habicht and Canfield, 1997), up to more regional scales within the water column (e.g. Newton et al., 2011). It is also possible to produce positive $\delta^{34}S$ values in the diagenetic environment (Jørgensen et al., 2004), and it has been suggested that stratigraphic accumulations (stratiform) of pyrite, with positive $\delta^{34}S$ values, may be diagnostic of sulphate reduction near the sulphate-methane transition zone (Borowski et al., 2013).

In the Selwyn Basin, Canada, a secular curve of $\delta^{34}S$ values (Fig. 1a) for barite ($\delta^{34}S_{barite}$) and pyrite ($\delta^{34}S_{pyrite}$) has been used to support a model in which high proportions of sulphate are reduced to sulphide in a restricted, euxinic water column (Goodfellow and Jonasson, 1984). In this model, positive $\delta^{34}S$ values of sulphate and sulphide develop according to closed system Rayleigh-type fractionation effects (Fig. 1b), coincident with three major periods of base metal mineralisation, previously described as sedimentary exhalative (SEDEX; Carne and Cathro, 1982). In the SEDEX model (Fig. 1c), venting of Pb–Zn–Fe ± Ba rich hydrothermal fluids into a stratified euxinic water column produces stratiform accumulations of base metal sulphides and barite (Goodfellow and Lydon, 2007). Therefore, a fundamental component of the SEDEX model is the generation of the reduced sulphur metal trap via a single step process (BSR) operating in the water column (Goodfellow, 1987). This necessitates a strong secular control on ore genesis with respect to periods of water column stagnation, which has been used to explain the distribution of SHMS deposits throughout the geological record (Goodfellow and Jonasson, 1984; Turner, 1992). However, there is reasonable doubt concerning the conventional interpretation of the isotopic record for barite and pyrite in the Selwyn Basin, for two reasons: (1) samples from SHMS systems are fine-grained and contain multiple generations of pyrite, and there is high potential for large isotopic heterogeneities on a small scale (e.g. Eldridge et al., 1988, 1993; Kelley et al., 2004a,b), and (2) for previous studies in the Selwyn Basin, poor spatial resolution between

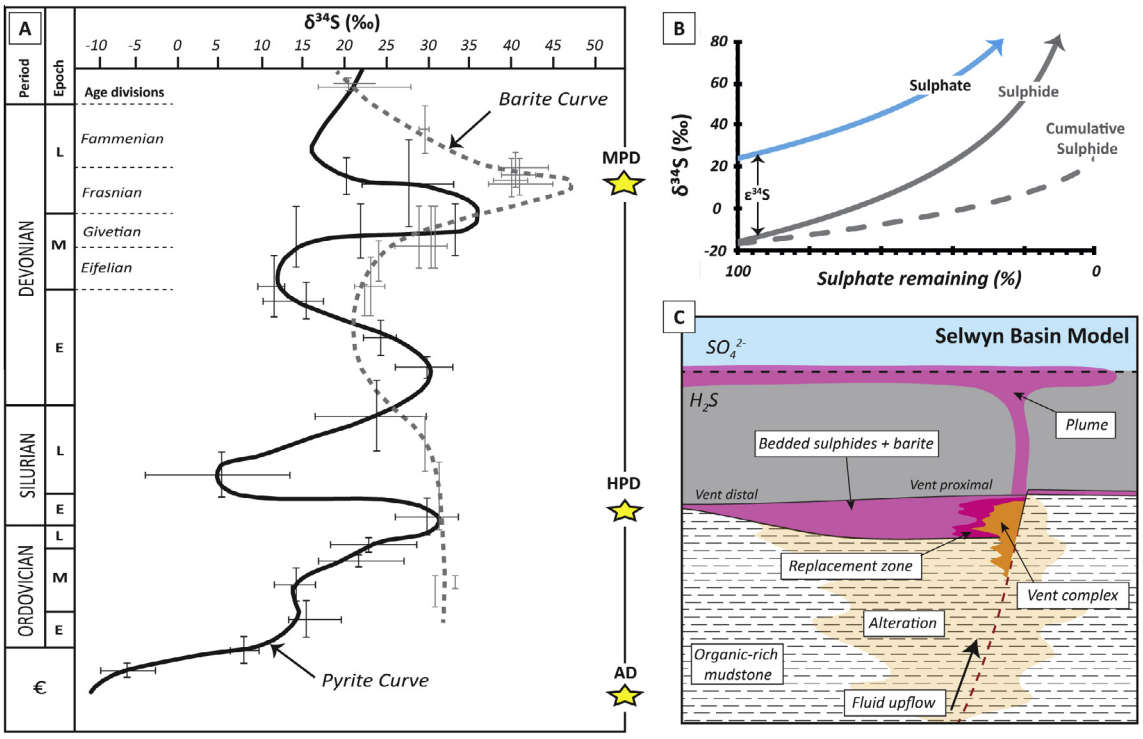

Fig. 1. (a) The Selwyn Basin sulphur isotope curve for barite (dashed grey line) and pyrite (solid black line); bars represent range of $\delta^{34}S$ values and uncertainty of age constraint (re-plotted from Goodfellow and Jonasson, 1984). The stars denote the location in the stratigraphy that hosts the Tom and Jason deposits of the Macmillan Pass District (MPD), Howards Pass District (HPD) and Anvil District (AD). Epochs are divided into Early (E), Middle (M) and Late (L), and relevant Devonian age divisions are annotated. (b) A schematic of closed-system, Rayleigh-type fractionation of sulphur isotopes during bacterial sulphate reduction ($\varepsilon^{34}S = 40$ ‰). The solid blue and grey lines track the evolution in $\delta^{34}S$ values of respective sulphate and sulphide; the dashed grey line represents the $\delta^{34}S$ value of total accumulated sulphide, which reaches the initial $\delta^{34}S$ value of sulphate (24 ‰) when no sulphate remains (i.e. 0%). (c) A schematic of the sedimentary-exhalative (SEDEX) style of mineralisation for the Selwyn Basin, where sulphide and barite precipitation occurs from a stratified, euxinic water column. The different components of the deposit architecture preserved at Tom and Jason are labelled. Samples in this study were obtained predominantly from the bedded mineralisation, where stratiform textures in sulphides and barite are well preserved. (For interpretation of the references to colour in this figure legend, the reader is referred to the web version of this article.)

samples of pyrite and barite mean the relationship between coeval $\delta^{34}S_{pyrite}$ and $\delta^{34}S_{barite}$ values is unclear (e.g. Goodfellow and Jonasson, 1984; Gardner and Hutcheon, 1985).

In this study, these issues have been addressed using *in situ* secondary ion mass spectrometry (SIMS) analysis of $\delta^{34}S_{pyrite}$, $\delta^{34}S_{barite}$ and $\delta^{18}O_{barite}$ values in samples from two Late Devonian SHMS systems (Tom, Jason) in the Selwyn Basin (Macmillan Pass; Fig. 1a). The SIMS data has been supplemented with analyses of bulk rock $\delta^{34}S_{pyrite}$ values, which provides a powerful tool with which to assess the relative contribution (i.e. the mass balance) of different sources of sulphur. Three main objectives have been addressed: (1) establish a comprehensive petrographic framework within which to interpret isotopic data, (2) constrain the environment of mineral formation, and (3) evaluate the mutual evolution of both sulphate and sulphide at Macmillan Pass to provide a more internally consistent understanding of sulphur cycling in these systems. The results presented in this study will be relevant to understanding how positive $\delta^{34}S_{sulphide}$ values develop in SHMS systems, and also marine strata from the geologic record.

2. SELWYN BASIN GEOLOGY

The Selwyn Basin, Canada, contains clastic rocks deposited in a passive margin setting along the western margin of North America between the late Neoproterozoic and Late Devonian (Gordey and Anderson, 1993). Paleozoic stratigraphy is dominated by organic-rich mudstones interpreted to represent deep-marine, pelagic sedimentation during periods of limited clastic input (Goodfellow and Jonasson, 1986; Goodfellow, 2007). These mudstones are host to three major periods of SHMS mineralisation during the Cambrian (Anvil District; Pigage, 1991), Silurian (Howard's Pass District; Morganti, 1979; Gadd et al., 2015) and Late Devonian (Macmillan Pass District; Gardner and Hutcheon, 1985; Ansdell et al., 1989). In the Late Devonian-Mississippian, Selwyn Basin strata were deformed during collision with an island arc, and incorporated into the Cordilleran fold and thrust belt (Nelson et al., 2006).

The metamorphic grade of Late Devonian strata at Macmillan Pass is considered to be sub-greenschist, and although no indicator minerals have been identified (McClay, 1991), conodont alteration indices of 5 provide

evidence that temperatures may have exceeded 300 °C during regional metamorphism (Irwin and Orchard, 1989; Gordey and Anderson, 1993). The Tom and Jason deposits have been deformed into tight, upright folds (Fig. 2), and the development of penetrative cleavage and pressure solution textures have been documented at both deposits (Bailes et al., 1986; McClay and Bidwell, 1986). However, at both deposits, the most intense deformation is located proximal to the fold hinges, and on the limbs of the folds many of the primary sedimentary and hydrothermal features are undeformed and well preserved. Thus, it is possible to reconstruct the complete deposit architecture at both Tom and Jason (e.g. Fig. 1c), comprising: (1) a discrete vent complex feeder zone, which forms a network of iron carbonate (ankerite, siderite) and sulphide stockwork style veins and alteration, (2) massive sulphide and barite mineralisation in a replacement zone proximal to the vent complex, and (3) laterally extensive, sulphide and barite bedded mineralisation.

The age constraints on the sulphur isotope curve (Fig. 1; Goodfellow and Jonasson, 1984) are provided by conodont biostratigraphy (Dawson and Orchard, 1982; Irwin and Orchard, 1991) and stratigraphic correlations (Gordey and Anderson, 1993). The assumption of the conventional SEDEX model is that mineralisation was syn-sedimentary, and therefore the deposits are considered to be of equivalent age to the host rock. At Macmillan Pass, conodont biostratigraphy for Macmillan Pass strata constrains the age of mudstones hosting the Tom and Jason deposits to between the Lower *hassi* through Lower *rhenana* conodont zones, corresponding with a Frasnian age (Fig. 1a). Studies of $\delta^{34}S_{CAS}$ values provide high resolution constraints for seawater sulphate, which during the Frasnian was between +20‰ and +25‰ (John et al., 2010; Chen et al., 2013). During the early part of the Frasnian, the CAS record is relatively stable; however, analyses across the Frasnian–Fammenian boundary record large shifts ($\delta^{34}S = +35‰$ down to +10‰; Chen et al., 2013).

3. SAMPLES AND ANALYTICAL METHODS

3.1. Samples

Samples were collected from drill-core located at the Tom and Jason deposits (Macmillan Pass, Yukon Territory). A total of 10 drill-holes were logged and sampled, and over 400 mineralised samples were collected. Care was taken to sample the least deformed examples of mineralisation, which preserve primary mineralogical relationships, and in particular, examples of stratiform barite, pyrite and ore-forming sulphides (e.g. Fig. 3). Paragenetic relationships were assessed under binocular microscope, and key samples were prepared as thin sections. Transmitted and reflected light petrography, and backscatter electron (BSE) imagery were used to assess the mineralogical relationships. Un-mineralised (barren) mudstone samples were also collected from two drill-holes (76-17, $n = 18$; TYK-5, $n = 19$): TYK-5 intersects approximately 40 metres of mineralised strata at the Tom deposit, and samples were obtained from above and below this mineralised sequence; 76-17 is located between the Tom and Jason deposits, intersects no mineralisation, and has been correlated with strata at Tom (see Magnall et al., 2015). The mudstone samples from both drill-holes preserve no visible indication of hydrothermal alteration, and although pyritic, they contain no other major sulphide phases. The barren mudstones are dark in colour and siliceous, and were collected from the same sedimentary sequence as in the previous study of Goodfellow and Jonasson (1984).

3.2. Secondary ion mass spectrometry (SIMS)

Sample preparation, pre-analysis imaging and isotopic analysis were performed at the Canadian Centre for Isotopic Microanalysis (CCIM), University of Alberta. Sample discs were isolated from polished thin sections using diamond core bits ranging between 2 and 3 mm diameter.

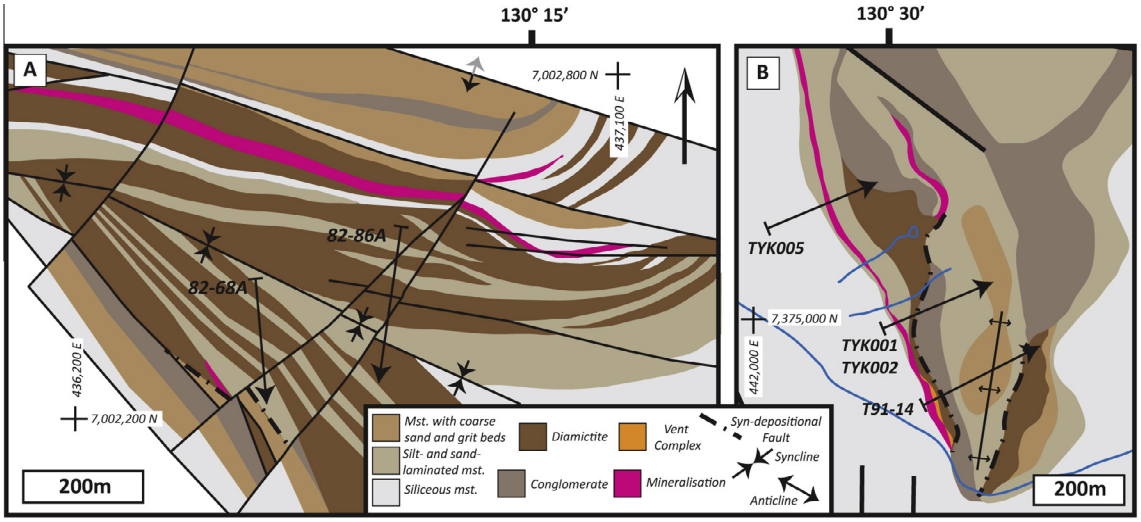

Fig. 2. The deposit geology at the Tom deposit (a), adapted from McClay and Bidwell (1986), and Jason deposit (b), adapted from Turner (1991). The approximate locations of drill-hole collars and plunge direction of drill-cores are denoted by the labelled arrows.

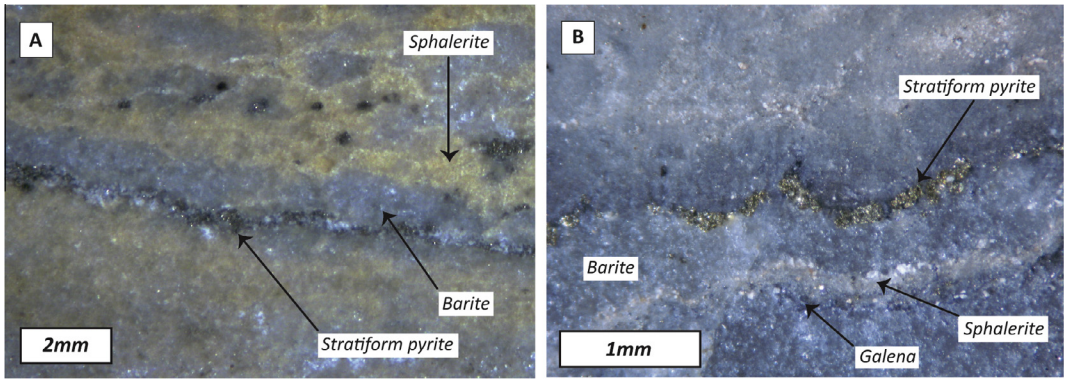

Fig. 3. Hand sample photographs of stratiform textures from the bedded mineralisation at Jason: in (a) stratiform pyrite and barite can be traced across the centre of the image, with sphalerite (orange) occurring as more irregular intergrowths to barite (81-68A; 716 metres); (b) irregular stratiform horizons of pyrite, sphalerite and galena within a barite-rich sample (81-68A; 784 metres). (For interpretation of the references to colour in this figure legend, the reader is referred to the web version of this article.)

The discs ($n = 40$) were cast in epoxy, along with pre-polished pieces of in-house barite (S0327) and pyrite (S0302A) reference materials (RM's) to form two standard 25 mm mounts (M1269 and M1270). The mounts were coated with 7 nm Au and imaged using a scanning electron microscope (SEM; Zeiss EVO MA15), operating at 20 kV and 3 nA beam current. Once imaged, mounts were coated with additional Au to bring the total to 30 nm.

Sulphur isotope ratios ($^{34}S/^{32}S$) and oxygen isotope ratios ($^{18}O/^{16}O$) were determined using an IMS-1280 multi-collector ion microprobe. The isotopic composition of sulphur and oxygen are reported in standard δ-notation, in reference to Vienna Canyon Diablo Troilite (V-CDT) for sulphur, and Vienna Standard Mean Ocean Water (V-SMOW) for oxygen. Key analytical conditions and parametres are summarised in Table 1. The primary beam used focused 20 keV $^{133}Cs^+$ ions to form a probe of 10–15 μm diameter. Negative secondary ions were extracted into the mass analyser, and automated tuning of the secondary preceded each analysis. Isotopes of interest ($^{32}S^-$, $^{34}S^-$, $^{16}O^-$, $^{18}O^-$) were analysed simultaneously in Faraday cups. The analytical protocol interspersed analyses of unknowns with the RM's in a 4:1 ratio. A total of 176 analyses of pyrite were performed, and 184 ($\delta^{34}S$) and 121 ($\delta^{18}O$) analyses of barite. Instrumental mass fractionation (IMF) was determined for the analytical sessions through evaluation of all the replicate analyses of the RM's. Final uncertainties are typically ±0.15‰ to 0.25‰ at a 95% confidence interval (2σ), and propagate within-spot counting errors, between-spot errors (geometric effects) and between-session errors. Errors do not include the absolute uncertainty in the composition of the RMs (Table 1) of ±0.2‰ to 0.5‰. The pyrite S0302A reference $\delta^{34}S_{VCDT}$ value was determined from SO_2 liberated by elemental analyser-continuous flow isotope ratio mass spectrometry techniques (EA-IRMS; University of Calgary, University of Leeds) and from fluorination and SF_6 measurements by dual inlet mass spectrometry (Massachusetts Institute of Technology). The barite S0327 reference $\delta^{34}S$ and $\delta^{18}O$ values were determined by EA-IRMS and dual inlet

Table 1
Variables in the operating conditions for SIMS analysis of $\delta^{34}S_{pyrite}$, $\delta^{34}S_{barite}$ and $\delta^{18}O_{barite}$ values.

	δ^{34}S-pyrite	δ^{34}S-barite	δ^{18}O-barite
Cs probe diameter (μm)	10	15	12
Beam current (nA)	0.85	2.5	2.5
Electron gun used	No	Yes	Yes
Implantation raster (μm)	18 × 18	20 × 20	20 × 20
Entrance and field apertures (μm, mm)	122, 5 × 5	122, 5 × 5	122, 5 × 5
Field magnification	100×	100×	100×
Energy slit	Full open	Full open	Full open
Detectors	L′2 (FC, $10^{10}\Omega$), FC2 (FC, $10^{11}\Omega$)	L′2 (FC, $10^{10}\Omega$), FC2 (FC, $10^{11}\Omega$)	L′2 (FC, $10^{10}\Omega$), H′2 (FC, $10^{11}\Omega$)
Mass resolution	2000, 2100	2000, 2100	1950, 2275
Secondary ions detected and mean counts/s	$^{32}S^- = 1 * 10^9$ $^{34}S^- = 4.5 * 10^7$	$^{32}S^- = 7 * 10^8$ $^{34}S^- = 3 * 10^7$	$^{16}O^- = 3.5 * 10^9$ $^{18}O^- = 7 * 10^6$
RM identity	S0302A pyrite	S0327 barite	S0327 barite
RM composition	$\delta^{34}S_{VCDT} = -0.2 \pm 0.2$‰	$\delta^{34}S_{VCDT} = +21.3 \pm 0.2$‰	$\delta^{18}S_{VSMOW} = +11.0 \pm 0.5$‰
Peak counting time	75 s	75 s	75 s
Standard deviation of RM analyses	0.04‰	0.05‰	0.07‰ – 0.11‰
Typical ± 2σ of unknowns	±0.17‰	±0.20‰	±0.24‰

methods (University of Calgary, University of Leeds), with $\delta^{18}O$ values referenced to NBS 127 = +8.6‰. All $\delta^{34}S$ pyrite and barite reference materials and measured values have been normalised to the same scale as the whole rock techniques (see below; the SO_2 method). Corrections for IMF are linear over a wide range of $\delta^{34}S$ and $\delta^{18}O$ values, as determined through evaluation of various in-house reference materials, and no orientation-related biases have been found for SIMS analysis of pyrite or barite at CCIM (e.g. Kozdon et al., 2010).

3.3. Bulk rock analysis of $\delta^{34}S_{pyrite}$ values

A chromous chloride extraction of pyrite sulphur was made using the technique of Canfield et al. (1986). The isotopic composition of the extracted sulphide, as Ag_2S, was analysed on an Isoprime mass spectrometer coupled to an Elementar Pyrocube elemental analyser. Samples were wrapped in tin cups and combusted with oxygen (N5.0) at 1150 °C in a stream of helium. The resulting gases were passed over tungstic oxide at the same temperature. Water was removed from the gas stream using phosphorus pentaoxide on an inert carrier (Sicapent) and excess oxygen was removed by passing the gas over copper wires held at 850 °C. SO_2 was separated from other gases using a temperature controlled adsorption/desorption column. The $\delta^{34}S$ value was derived using the integrated mass 64 and mass 66 signals from the sample relative to those in a pulse of independently introduced reference gas (N3.0). All solid reagents were sourced from Elemental Microanalysis, UK, and all gases from BOC, UK. Calibration to the international scale was performed using IAEA-S3 and an in house seawater sulphate standard (SWS-3) isotopically indistinguishable from NBS-127. The SWS-3 BaSO4 seawater standard was calibrated (using the IAEA quoted values) against S1, S3, NBS-127 & NBS-123. The values we used for this calibration are: NBS-127 = +20.30‰, NBS-123 = +17.01‰, IAEA S-1 = −0.30‰ and IAEA S-3 = -32.06‰. Errors (1σ) are reported as 0.17‰ and 0.40‰ for samples from 76-17 and TYK-5 respectively, representing the average standard deviation of analyses of the two standards.

4. RESULTS

4.1. Mineralogical paragenesis

The mineralogical paragenesis can be split into three stages (Fig. 4), two of which precede hydrothermal input (as recorded by sphalerite and galena formation). The barren mudstone samples from 76-17 and TYK-5 contain pyrite from stages 1 and 2, and no barite, whereas samples from the bedded mineralisation contain all 3 paragenetic stages. Key features of the paragenesis will now be described in chronological order.

Stage 1. Framboidal pyrite (py-1) is a distinctive early phase (Fig. 5a), with individual framboids mostly greater than 7 μm in diameter (often >20 μm). An early generation of barite (brt-I) forms small (<25 μm), interstitial, anhedral crystals that typically occur as patchy replacements of quartz within mudstone beds (Fig. 5b). The temporal relationship between py-I and brt-I is hard to distinguish, as they rarely appear intergrown together. Radiolarians represent an original biogenic component of the host rock, which are preserved by authigenic carbonate, silica and also later hydrothermal pyrite (see Magnall et al., 2015). Notably, radiolarian tests preserved by Stage 3 sulphides (galena, sphalerite, pyrite) can be locally enriched in microscopic barium (Fig. 5c and d).

Stage 2. Euhedral pyrite (py-II) post-dates py-I in all samples (Figs. 5a and 6a) and is present in two main forms, as either stratiform accumulations (py-IIa; Figs. 3 and 6a)

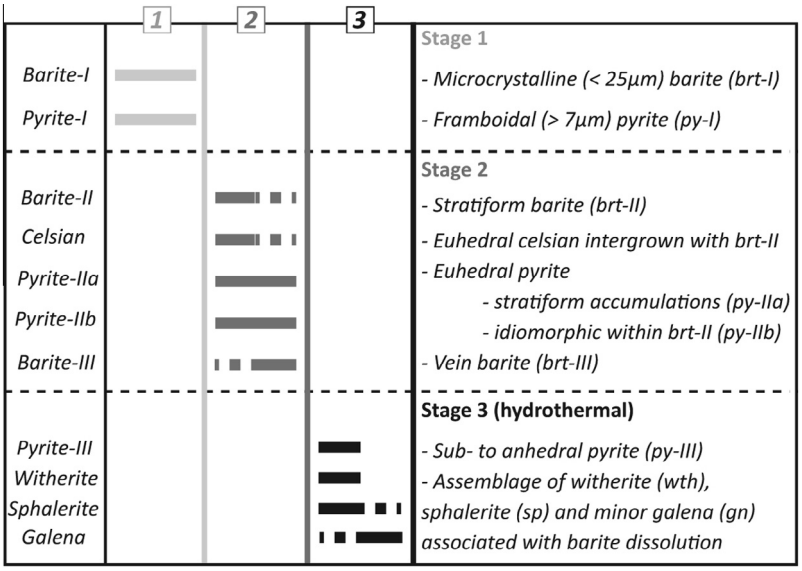

Fig. 4. Mineralogical paragenesis for mineralised samples at Tom and Jason. Stages 1 and 2 predate the hydrothermal mineralisation (Stage 3). Dashed lines reflect uncertainty in the timing relationships.

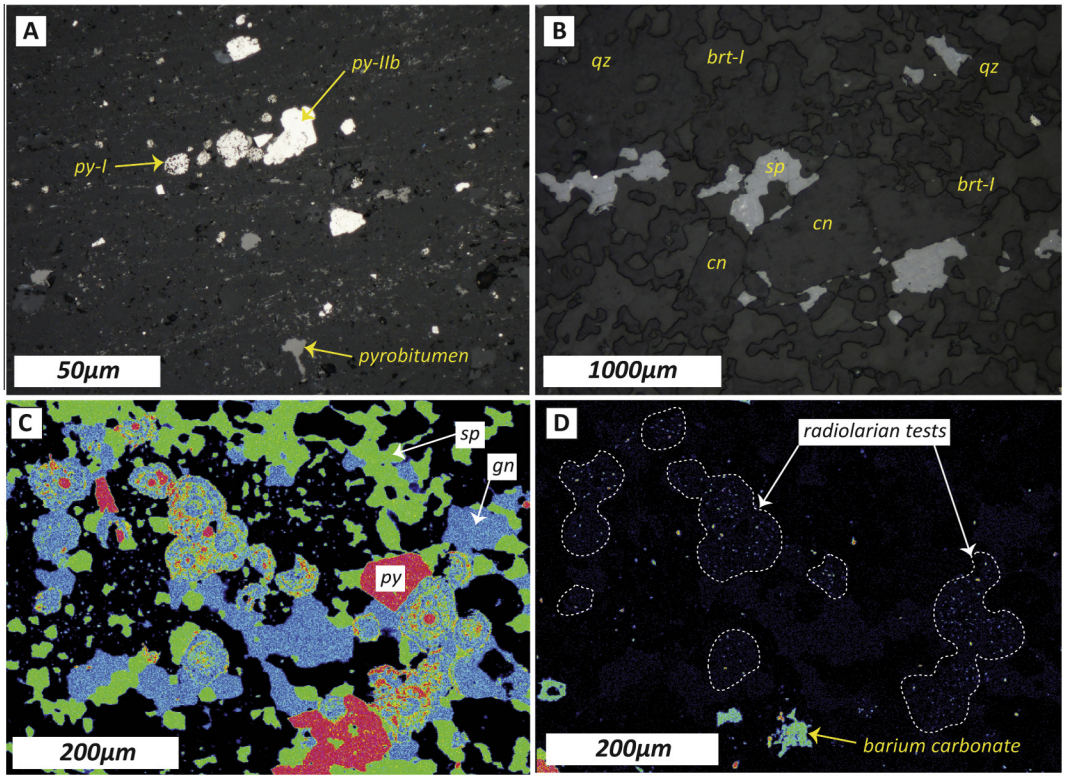

Fig. 5. (a) A reflected light photomicrograph of framboidal py-I, overgrown by euhedral py-IIb, in an un-mineralised (barren) mudstone sample from 76-17 (279.6 metres). (b) A reflected light image of barite (brt-I) interstitial to microcrystalline quartz (qz) from T91-14 (21 metres). Barium feldspar (celsian; cn) occurs in the centre of the image, partially replaced by barite. Sphalerite (sp) occurs as interstital replacement of barite. (c) Electron microprobe X-ray imaging of sulphur in a sample of bedded mineralisation from T91-14 (36 metres), where green = sphalerite, red = pyrite, and blue = galena. (d) The same sample as in (c), imaged for barium, which corresponds with light blue colours. Note the localised micron scale enrichments within the skeletal structure of the radiolarians. The larger, Ba-bearing, anhedral crystals at the bottom of the image do not contain sulphur, and are therefore likely barium carbonate. (For interpretation of the references to colour in this figure legend, the reader is referred to the web version of this article.)

or as solitary, disseminated crystals (py-IIb; Fig. 6a and b). Separating py-IIa and py-IIb temporally within stage 2 has not been possible. Barite-II (brt-II) forms more equant, euhedral crystals (>25 µm; Fig. 6b), which often occur as discontinuous stratiform enrichments in association with py-IIa (Fig. 3). There can be a continuum of textures between brt-I and brt-II, and the patchy brt-I enrichments (stage 1) sometimes develop into the more monominerallic, stratiform brt-II. Commonly, py-IIb occurs intergrown with brt-II (Fig. 6b). Barite-III (brt-III) is present as irregular veinlets that crosscut mudstone laminae and earlier barite generations, but which also occurs as feeder veins linked to the formation of brt-I and brt-II (Fig. 6c). Euhedral, monoclinic celsian crystals provide a useful marker phase in the paragenesis, often occurring on the top of mudstone laminations, along organic-rich horizons (e.g. Fig. 6b), and as overgrowths of py-I (Fig. 6d) and intergrown (but out of textural equilibrium) with brt-II (e.g. Fig. 5b).

Stage 3. This is a simple mineral assemblage, comprising pyrite, sphalerite, galena, and witherite, which characterises the hydrothermal input in the mineralised samples. Pyrite (py-III) forms large sub-to anhedral replacements and overgrowths of earlier barite (Fig. 6e), and witherite forms an accessory phase to sphalerite (Fig. 6e). Galena is the last phase in the paragenesis, and occurs as anhedral, interstitial crystals that replace earlier barite and pyrite mineralisation along stratiform horizons (Fig. 6f).

4.2. SIMS – sulphur and oxygen isotopes

The $\delta^{34}S$ values for both barite and pyrite are summarised in Fig. 7 (see electronic Appendix for full compilation). Pyrite-I preserves very negative $\delta^{34}S$ values, between −30.0‰ and −20.8‰. Despite being texturally distinct, subsequent generations of pyrite (py-II + III) have an overlapping distribution of $\delta^{34}S$ values between +3.0‰ and +25.7‰. Barite preserves $\delta^{34}S$ values between +22.5‰ and +33.0‰, and the three generations of barite are isotopically indistinct; however, there are large isotopic variations (3–4‰) recorded on a very small scale (<50 µm) within barite of the same generation. The $\delta^{18}O$ values of barite are between +16.4‰ and +18.3‰, and are presented in a cross plot with $\delta^{34}S$ values in Fig. 8.

For brt-II and py-II, there are some important isotopic relationships to highlight: (1) $\delta^{34}S$ values of the stratiform pyrite (py-IIa; +17.4‰ to +25.7‰) and barite (brt-II; +22.7‰ to +29.6‰) approach isotopic equivalence (i.e.

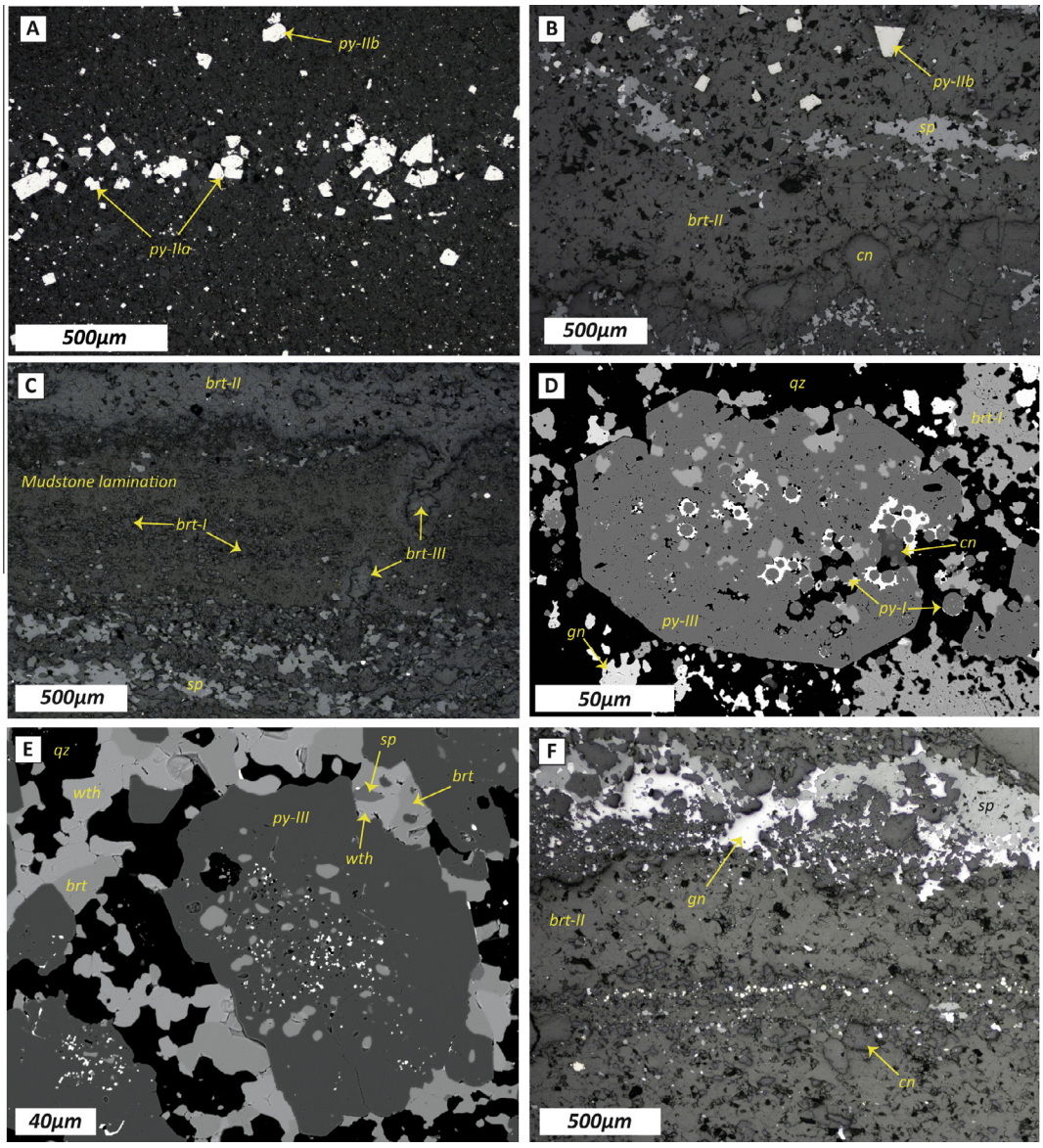

Fig. 6. (a) A reflected light image of stratiform pyrite (py-IIa) in a barren mudstone sample from TYK-5 (90 metres). (b) A reflected light image of a sample from TU-68 (3 metres), showing barium feldspar (celsian; cn) formed along a stratiform horizon, with euhedral barite (brt-II) overlying and replacing it. Euhedral py-IIb crystals occur within brt-II and are overgrown by subsequent sphalerite (sp) in the upper left hand portion of the image. (c) A reflected light image of a sample from TYK-1 (22 metres), where a mudstone lamination with interstitial barite (brt-I) is interlaminated with brt-II and crosscut by brt-III. Sphalerite (sp) replaces barite towards the bottom of the image. (d) A back-scatter electron (BSE) image of framboidal pyrite (py-I) and barite (brt-I) overgrown by a later generation of pyrite (py-III); py-I appears to provide a porous framework for the hydrothermal fluid, which is highlighted by the formation of galena around individual framboids. Sample is from T91-14 (21 metres). (e) A BSE image of Stage 3 pyrite (py-III), sphalerite (sp) and witherite (wth) replacing barite (brt). (f) A reflected light image showing stratiform brt-II replaced by sphalerite (sp) and galena (gn). Both (e) and (f) are images of a sample from TYK-2 (27 metres).

$\delta^{34}S_{pyrite} \approx \delta^{34}S_{barite}$), and (2) idiomorphic pyrite (py-IIb) in textural equilibrium with brt-II (e.g. Fig. 6b) preserve median $\Delta^{34}S$ values of +15‰.

4.3. Bulk rock $\delta^{34}S_{pyrite}$ values

The $\delta^{34}S$ values of sulphur extracted from barren mudstone samples (drill-holes 76-17 and TYK-5) can be assumed to originate from pyrite, owing to the absence of hydrothermal sulphides (sphalerite, galena). Bulk rock $\delta^{34}S_{pyrite}$ values (Fig. 6) form a broad distribution, from −15.6‰ to +8.7‰ ($n = 37$). The data from the two different drill-holes form overlapping distributions of $\delta^{34}S$ values: in 76-17, $\delta^{34}S$ values are between −15.6‰ and −0.7‰, whereas in TYK-5, values are between −5.3‰ and +8.7‰. Although these samples were obtained from the same stratigraphic interval as those analysed by Goodfellow and Jonasson (1984), data in this study extend

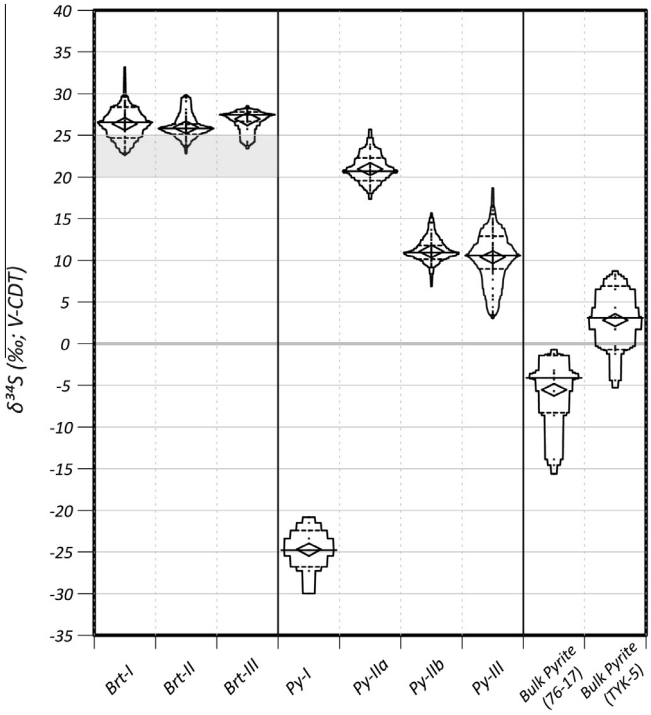

Fig. 7. The $\delta^{34}S$ values for barite and pyrite presented as box percentile plots, with distribution shape., along with statistical data. Black dots represent individual analyses, diamonds represent mean values, solid horizontal lines represent median values and dashed horizontal lines provide the 25th and 75th percentiles. Mineral phases are indicated below. Grey box represents $\delta^{34}S$ value of Late Devonian seawater sulphate (John et al., 2010; Chen et al., 2013).

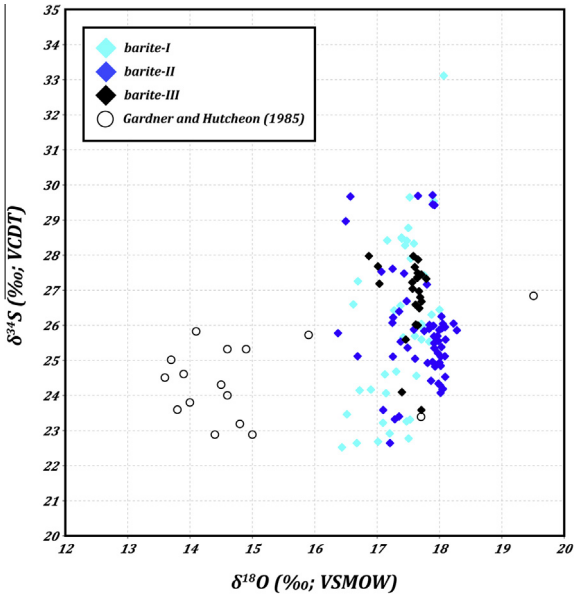

Fig. 8. Plot of $\delta^{18}O$ against $\delta^{34}S$ values for barite in Late Devonian strata at Macmillan Pass, including data from Gardner and Hutcheon (1985).

to much lower $\delta^{34}S$ values (−15.6‰ to +8.7‰; this study, *versus* +22.0‰ to +33.8‰; Goodfellow and Jonasson, 1984).

5. DISCUSSION

In this study multiple generations of pyrite have been documented in both the bedded mineralisation at Macmillan Pass, and also barren mudstones from drill-holes 76-17 and TYK-5 (Figs. 5a and 6a). To understand where pyrite formed (water column or sediment) and the processes responsible for the distribution of $\delta^{34}S_{pyrite}$ values at Macmillan Pass (Fig. 7), it is first necessary to evaluate the spatial and temporal variability of coeval $\delta^{34}S$ values in sulphate, as preserved in barite ($\delta^{34}S_{barite}$).

5.1. Interpreting the isotopic composition of barite

5.1.1. $\delta^{34}S_{barite}$ values

The distribution of $\delta^{34}S_{barite}$ values (+22.5‰ to +33.0‰; Fig. 7) is very similar to previous mineral separate analyses of barite from the Tom and Jason deposits (+21.2‰ to +32.7‰, Goodfellow and Jonasson, 1984; +22.9‰ to +26.8‰, Gardner and Hutcheon, 1985). The exact location of sampling in the earlier studies is not clear; nevertheless, the general agreement of $\delta^{34}S_{barite}$ values provides good evidence that the data acquired via microanalytical techniques (this study) is representative of variability sampled at a broader scale (previous work).

In the Selwyn Basin model, stratiform textures are considered to result from syn-sedimentary processes, and $\delta^{34}S_{barite}$ values in excess of coeval Late Devonian seawater (>25‰; John et al., 2010) represent the effects of closed system, Rayleigh-type fractionation (e.g. Fig. 1c). However,

the bacterial reduction of seawater sulphate during diagenesis means that barite precipitated in this environment can also inherit $\delta^{34}S$ values that deviate from coeval seawater (e.g. Torres et al., 1996). With this caveat, only the lowest $\delta^{34}S_{barite}$ values should be compared directly with coeval seawater sulphate (Cecile et al., 1983). Notably, the lowest $\delta^{34}S_{barite}$ values reported at Macmillan Pass overlap with constraints for un-modified Frasnian seawater (+20‰ to +25‰; John et al., 2010; Chen et al., 2013). The preservation of $\delta^{34}S_{barite}$ values greater than +25‰ is evidence that some modification of seawater sulphate occurred; however, this is not unique to complete restriction of the sulphate reservoir (i.e. closed system), and can also be produced during barite precipitation from pore fluids open to diffusional exchange with the overlying water column (i.e. open system conditions where sulphate resupply >sulphate consumption). Indeed, barite at Macmillan Pass is generally greater than 5 μm in diameter, which is typical of barite precipitated beneath the SWI (Paytan et al., 2002).

Interestingly, the preservation of small-scale isotopic heterogeneities (3–4‰ over <50 μm) between individual brt-I crystals does provide evidence of transient changes in the rates of sulphate diffusion and consumption within pore fluid microniches (Widerlund et al., 2012); however, there is no convincing evidence that more positive $\delta^{34}S$ values developed in barite from later paragenetic stages (e.g. brt-III; Fig. 6). This overlap in $\delta^{34}S$ values between different barite generations suggests they were not temporally or even spatially (e.g. sediment depth) distinct, but that precipitation occurred from pore fluids with similar $\delta^{34}S$ values. Overall, there is no evidence of major contraction of the sulphate reservoir occurring via BSR, such that highly positive $\delta^{34}S$ values (>+40‰) were preserved during the precipitation of barite.

5.1.2. Relationship between $\delta^{34}S$ and $\delta^{18}O$ values in barite

As with sulphur, oxygen also undergoes a kinetic isotope fractionation during BSR (Mizutani and Rafter, 1973), which can result in a linear correlation between $\delta^{18}O$ and $\delta^{34}S$ values in the residual sulphate reservoir (e.g. Aharon and Fu, 2000). Unlike sulphur, oxygen isotopes can also be modified by equilibrium exchange between BSR reaction intermediaries (sulphate-enzyme complexes or SO_3^{2-}) and H_2O (Fritz et al., 1989; Wortmann et al., 2007). Therefore, in the geologic record there is potential to preserve variable relationships between $\delta^{18}O$ and $\delta^{34}S$ values in sulphate, depending on the relative contribution of kinetic *versus* equilibrium effects (Antler et al., 2013; Wankel et al., 2014).

In this study, $\delta^{18}O_{barite}$ values form a narrow distribution (+16.3‰ to +18.3‰; Fig. 8), albeit at more positive values relative to coeval seawater sulphate (+10‰ to +16‰; John et al., 2010). The only previous study of $\delta^{18}O$ and $\delta^{34}S$ values for Macmillan Pass barite (Gardner and Hutcheon, 1985) reported mostly lower $\delta^{18}O$ values, which overlap coeval seawater sulphate (Fig. 8). If the analyses of Gardner and Hutcheon (1985) are evaluated with the data from this study, an initial increase in $\delta^{18}O$ values (with invariant $\delta^{34}S$ values) is followed by an increase in $\delta^{34}S$ values (with relative invariance of $\delta^{18}O$ values). This is in contrast to other studies of barite (Johnson et al., 2004, 2009) where a positive trend between $\delta^{18}O$ and $\delta^{34}S$ values is often preserved. There is not a clear explanation for the $\delta^{18}O$ and $\delta^{34}S$ values in barite at Macmillan Pass; the relatively narrow range of $\delta^{34}S$ values, which suggests open system diffusional exchange with the overlying water column (Section 5.1.1.), might be expected to have similar implications for $\delta^{18}O$ values. Alternatively, the upper limit of $\delta^{18}O_{barite}$ values could also be a function of an equilibrium isotope-exchange effect (e.g. Antler et al., 2013; Wankel et al., 2014).

5.2. Origin of barium

The general mineralogical paragenesis at Macmillan Pass (Fig. 4), where barite predates all direct evidence of hydrothermal input (as represented by py-III, sphalerite and galena), suggests that processes responsible for barium transport and barite precipitation may have been decoupled from the Zn and Pb sulphide formation. This has also been recognised in the Red Dog district (Alaska), where textural (Kelley et al., 2004a,b) and isotopic (Johnson et al., 2004, 2009) studies support a diagenetic origin for barite. The important question, therefore, relates to how barium was concentrated into mudstones as barite in these settings.

Biological activity (and biogenic input) has been well constrained during deposition of the host rock, both at Macmillan Pass (Magnall et al., 2015) and in the Red Dog district, Alaska (Kelley et al., 2004a; Reynolds et al., 2015). Previous studies have proposed a correlation between barium enrichment in mudstones and paleoproductivity (Schmitz, 1987; Dymond and Collier, 1996; Paytan and Griffith, 2007), and there is evidence of an association between discrete barite particles (<1 μm) and planktonic organisms in modern day oceanographic settings (Dehairs et al., 1980; Bishop, 1988). This has also been replicated in laboratory experiments, in which barite precipitation has been biologically mediated (Gonzalez-Munoz et al., 2012). At Macmillan Pass, radiolarian tests have been uniquely preserved as a result of hydrothermal sulphide precipitation, which occurred before the diagenetic transformation of opaline silica to quartz. Notably, local enrichments of barium within the radiolarian tests provide evidence of a primary biologically mediated flux of barium (Fig. 5c and d).

These primary features are rarely preserved in the sedimentary record (e.g. Stamatakis and Hein, 1993), due to the diagenetic recycling of barite. Following the progressive consumption of pore fluid sulphate during BSR, any remaining labile organic matter will continue to degrade via methanogenesis (Froelich et al., 1979; Jørgensen and Kasten, 2006);

$$2CH_2O \rightarrow CO_2 + CH_4 \quad (1)$$

Reaction (1) may proceed via either biogenic (e.g. Joye et al., 2004) or thermogenic (e.g. Cruse and Seewald, 2006) processes, and both represent important pathways in the sedimentary carbon cycle (Jørgensen and Kasten, 2006). The methane, and other short-chain hydrocarbons produced during reaction (1) accumulate within late diagenetic, reducing pore fluids, which are highly effective at

enhancing barite solubility (Torres et al., 1996). The preservation of barite veins (brt-III; Fig. 6c) is consistent with studies that have documented barite dissolution and barium mobilisation in sulphate deficient pore fluids that develop during diagenesis (Torres et al., 1996; Dickens, 2001).

When opposing diffusional fluxes of methane and sulphate interact, anaerobic oxidation of methane (AOM) proceeds according to reaction (2) (Barnes and Goldberg, 1976; Reeburgh, 1976);

$$CH_4 + SO_4 \rightarrow HCO_3^- + HS^- + H_2O \quad (2)$$

A microbial consortium of syntrophic anaerobic methanotropic archaea (ANMEs) and sulphate reducers are thought to mediate this reaction (Hoehler et al., 1994; Knittel and Boetius, 2009), which can result in the development of a sharp redox boundary called the sulphate-methane transition zone (SMTZ; Iversen and Jørgensen, 1985). The SMTZ forms an important location of both diagenetic barite precipitation (e.g. Torres et al., 2003; Arndt et al., 2009; Henkel et al., 2012), and also reduced sulphur production and pyrite formation (Neretin et al., 2004).

5.3. Distribution of $\delta^{34}S$ values in pyrite ($\delta^{34}S_{pyrite}$)

Three major generations of pyrite (py-I, II, III) have been identified at Macmillan Pass (Fig. 4). Notably, the two earliest generations of pyrite preserve distinctive positive and negative end-member $\delta^{34}S$ values (see Fig. 7). Previous work has reported $\delta^{34}S_{pyrite}$ values between +22.0‰ and +33.8‰, acquired from analyses of mineral separates (Goodfellow and Jonasson, 1984). In this study, the most positive $\delta^{34}S_{pyrite}$ values are associated with stratiform pyrite (py-IIa), and it is possible that previous workers preferentially sampled this generation of pyrite. In the following section, the development of $\delta^{34}S_{pyrite}$ values will be considered within the framework of the $\delta^{34}S_{barite}$ values (Section 5.1), to evaluate how reduced sulphur was generated in the Late Devonian mudstones at Macmillan Pass.

5.3.1. Py-I (framboidal pyrite)

This generation of pyrite is disseminated throughout both the un-mineralised mudstones and bedded mineralisation at Macmillan Pass. Framboidal pyrite is thought to precipitate rapidly in aqueous solutions, when the precursors to pyrite formation, iron monosulphides, become supersaturated, i.e. sulphide production < iron supply (Raiswell, 1982; Passier et al., 1997). The $\delta^{34}S$ values preserved in py-I (−28.8 to −19.6‰; Fig. 7) represent a large offset from the $\delta^{34}S$ value of coeval sulphate ($\Delta^{34}S \leqslant 60‰$), corresponding with a large isotopic fractionation. Such large fractionations are typical of slower rates of BSR (Harrison and Thode, 1958; Kaplan and Rittenberg, 1964) and disproportionation (Canfield and Thamdrup, 1994). Slower rates of BSR have also been linked to higher rates of equilibrium oxygen isotope exchange (Deusner et al., 2014); therefore, the large fractionation associated with $\delta^{34}S_{py\text{-}1}$ and the narrow distribution of $\delta^{18}O_{barite}$ values (possibly a function of equilibrium exchange; Section 5.1.2.) forms complimentary evidence of diagenetic pore fluids undergoing slow rates of BSR. This also provides further supporting evidence that pore fluids represented a relatively open system, i.e. sulphate resupply > sulphate consumption. These results could also be produced in an open system (ventilated), euxinic water column (e.g. Lyons, 1997); however, this is not supported by the size of the majority of framboids (> 7 μm in diameter), which are consistent with precipitation beneath the SWI (Wilkin et al., 1996).

5.3.2. Py-II (euhedral pyrite)

Texturally, py-II forms the clearest paragenetic relationship with barite (brt-II), either as stratiform accumulations (py-IIa; Fig. 3) or intergrown with brt-II (py-IIb; Fig. 6b). The euhedral morphology of py-II probably represents a decrease in the level of pore fluid supersaturation with respect to iron monosulphides, resulting from limited iron or sulphate supply (Raiswell, 1982; Passier et al., 1997). The Stage 2 mineral assemblage clearly pre-dates hydrothermal input, and importantly, py-IIa preserves the highest $\delta^{34}S$ values. However, as discussed previously (Section 5.1.1.), there is no evidence of a substantial reservoir effect in the relatively narrow range of $\delta^{34}S_{barite}$ values, even for barite in close proximity to py-IIa (e.g. Fig. 9). Indeed, this isotopic relationship is not consistent with regional Rayleigh-type fractionation in a euxinic water column (i.e. Selwyn Basin model; Fig. 1c). The intergrown relationship between py-IIb and brt-II (e.g. Fig. 6b) is such that, assuming coeval precipitation from the same diagenetic fluid, the isotopic relationship may be a good approximation of the actual fractionation associated with sulphate reduction during Stage 2 (i.e. $\Delta^{34}S_{brt-py} \approx \varepsilon^{34}S < 15‰$). This represents a major decrease from the isotopic fractionation associated with the formation of py-I.

As samples from this study have been affected by hydrothermal processes, it is necessary to evaluate the potential role of thermochemical sulphate reduction (TSR), by which it is possible to generate positive $\delta^{34}S_{sulphide}$ values (Machel et al., 1995). Above 110 °C and in the presence of a reductant (e.g. organic matter), sulphate can be reduced with an associated kinetic fractionation that scales with temperature (Kiyosu and Krouse, 1990). Using the experimentally derived equation of Kiyosu and Krouse (1990), the isotopic relationship between brt-II and py-IIa ($\Delta^{34}S_{brt-py} < 10‰$) would have required temperatures in excess of 250 °C. Alternatively, it may be that the entire budget of sulphate was consumed during TSR, in which case $\delta^{34}S_{sulphide}$ could approach $\delta^{34}S_{sulphate}$ values. In both scenarios, major barite dissolution should be associated with the formation of py-IIa, to provide a source of sulphate; however, there is no textural evidence of this in the relationship between py-IIa and brt-II (e.g. Fig. 6b). Furthermore, carbonate, which is an important by-product of TSR (see Machel et al., 1995; Machel, 2001), is also absent in the Stage 2 assemblage (see Table 2). Rather than forming via TSR, the positive $\delta^{34}S_{pyrite}$ values were more likely generated during diagenesis, which is also consistent with the occurrence of py-II in the un-mineralised mudstone samples (Fig. 5a and 6a). Stratiform pyrite (and mineralogical precursors) has been recognised in diagenetic settings (e.g. Kasten et al., 1998), and in studies

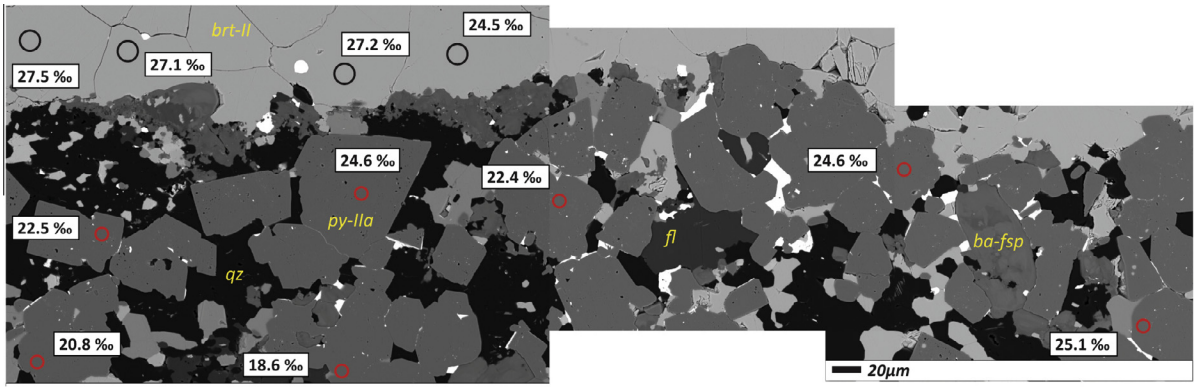

Fig. 9. A compilation of backscatter electron images of a stratiform horizon of py-IIa and brt-II, annotated with $\delta^{34}S$ values.

Table 2
Summary of features for non-hydrothermal pyrite at Macmillan Pass, and their calculated contribution to the bulk rock signature in 76-17 and TYK-5.

	Morphology	$\delta^{34}S$ (‰)	Reduced S pathway	Setting	% Contribution to 76-17	% Contribution to TYK-5
Py-I	Framboidal	−20.8 to −30.0	BSR	Below SWI	35–55	35–15
Py-IIa	Euhedral	+17.4 to +24.7	AOM-SR	Below SWI	45–65	65–85
Py-IIb	Euhedral	+6.9 to +15.7	AOM-SR/BSR	Below SWI		
G+J (1984)		+22.0 to +33.8	BSR	Water Column		

of modern day sapropels where pyrite typically accumulates along centimetre thick horizons (Passier et al., 1997). The stratiform pyrite forms when upwardly diffusing Fe^{2+} encounters bisulphide generated during sulphate reduction, which at the SMTZ can occur in near quantitative proportions (Niewöhner et al., 1998). Importantly, this can result in formation of highly positive $\delta^{34}S_{pyrite}$ values (Jørgensen et al., 2004; Borowski et al., 2013). We would argue, therefore, that where stratiform accumulations of py-IIa and brt-II are preserved at Macmillan Pass (e.g. Figs. 3 and 9) they represent a relict SMTZ (see model in Fig. 10).

In modern day environments, the SMTZ has been located between 1.5 metres (Iversen and Jørgensen, 1985; Niewöhner et al., 1998) and depths exceeding 8 metres below the SWI (e.g. Borowski et al., 2013). The main factors contributing to the location of the SMTZ within a sedimentary sequence include the rate of organic carbon remineralisation (BSR and methanogenesis), sedimentation rate and sulphate concentration (Jørgensen et al., 2004; Arning et al., 2015). During the Late Devonian, lower concentrations of sulphate in seawater (7 mM; Horita et al., 2002), may well have resulted in reduced sulphate penetration beneath the SWI, resulting in a SMTZ closer to the seafloor. This has important implications for the interpretation of the $\delta^{34}S$ values of barite and pyrite. Specifically, the isotopic relationship between brt-II and py-II (e.g. Fig. 9) records no evidence of a substantial reservoir effect ($\delta^{34}S_{barite} \gg 30‰$). This may appear counterintuitive, considering that as sulphate concentrations decrease towards the SMTZ, the system should become more susceptible to closed system Rayleigh-type effects. However, the reduced isotopic fractionation associated with Stage 2 pyrite formation ($\varepsilon^{34}S < 15‰$) would also have influenced how $\delta^{34}S$ values in the coeval sulphate reservoir evolved (e.g. Jones and Fike, 2013). Indeed, open system conditions and reduced isotopic gradients have been documented where SMTZs form in proximity to the seafloor (e.g. Jørgensen et al., 2004; Borowski et al., 2013). This has been modelled in Fig. 11, which illustrates how $\delta^{34}S$ values in sulphate and sulphide may have evolved in an open system, where Stages 1 and 2 correspond with respective $\varepsilon^{34}S$ values of 54‰ and 10‰. Clearly, if the majority of reduced sulphur is produced during Stage 2, the development of highly positive $\delta^{34}S_{barite}$ values will not occur (dashed line of Stage 1 in Fig. 11), which is consistent with the distribution of $\delta^{34}S_{barite}$ values preserved in the bedded mineralisation at Macmillan Pass.

5.3.3. Bulk rock $\delta^{34}S_{pyrite}$ values

As established for the mineralised samples, $\delta^{34}S_{pyrite}$ values provide evidence of reduced sulphur generation during two stages of pyrite formation (py-I and py-II), linked to BSR and AOM-SR. These two stages of pyrite have also been identified in barren mudstones. Thus, the relative contribution of reduced sulphur sourced from different generations of pyrite can be evaluated from bulk rock analyses of $\delta^{34}S_{pyrite}$ values in barren mudstones. A binary mixing model has been used to assess the relative contributions of py-I and py-II to the reduced sulphur budget of the host mudstones. In 76-17, to account for the bulk rock isotopic composition (between 25th and 75th percentiles), py-II contributes 45-65% of the reduced sulphur budget; however, for TYK-5 this value is greater, between 65% and 85% (see Table 2). Importantly, TYK-5 is a drill-hole that intersects approximately 40 metres of bedded mineralisation at the Tom deposit (Magnall et al., 2015). It has been shown that

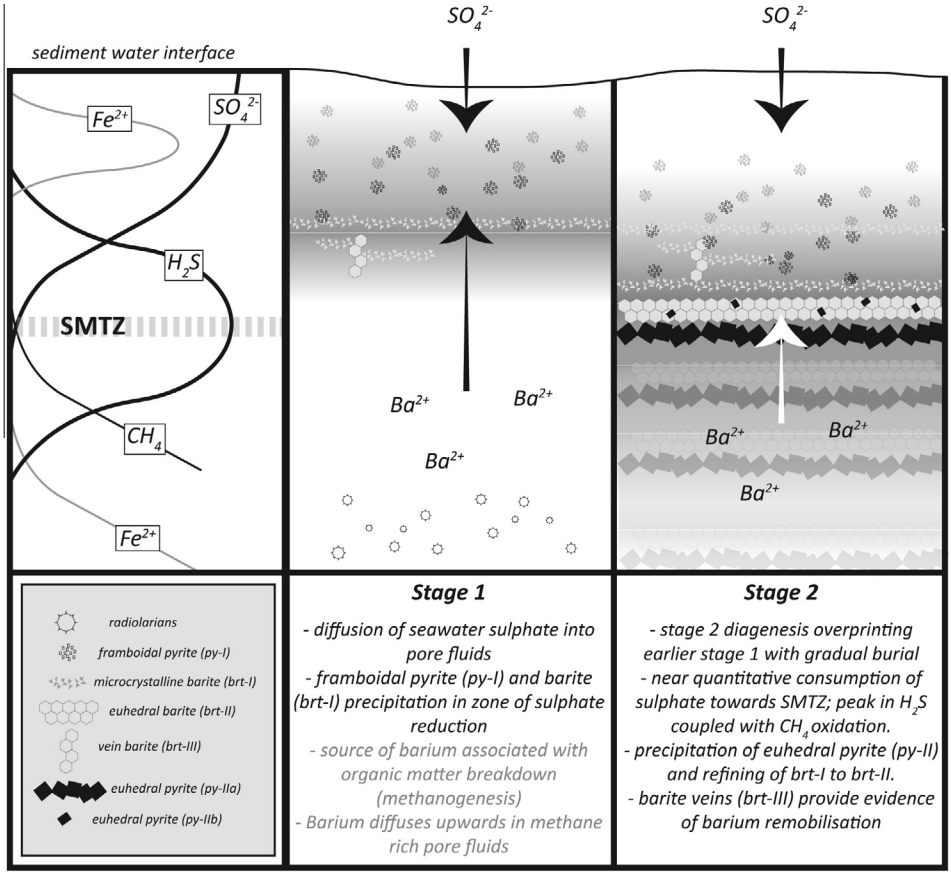

Fig. 10. A schematic model for the formation of Stages 1 and 2 of the mineralogical paragenesis at Macmillan Pass. The pore water profiles of key geochemical parameters (e.g. SO_4^{2-}, Fe^{2+}, CH_4 and H_2S) are given on the left hand side. The sulphate methane transition zone (SMTZ) occurs where diffusional gradients of sulphate and methane intersect, resulting in peak concentrations of reduced sulphur.

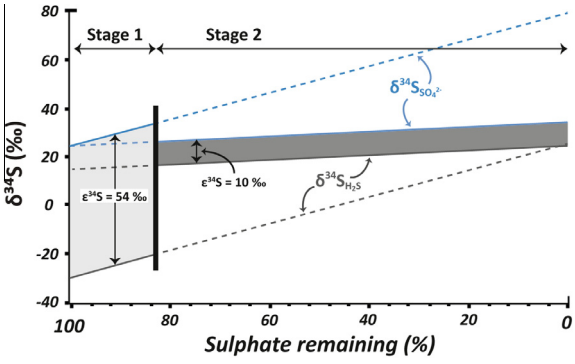

Fig. 11. The respective evolution of $\delta^{34}S$ values in both barite and pyrite from Stages 1 and 2, modelled for open system conditions. The dashed lines represent the trends for $\delta^{34}S$ values that are not preserved in barite or pyrite. The model shows that during Stage 2, a reduced isotopic fractionation ($\varepsilon^{34}S = 10‰$) associated with sulphate reduction results in a suppressed isotopic gradient in $\delta^{34}S_{barite}$. A greater proportion of reduced sulphur generated during Stage 2 can therefore explain the distribution of $\delta^{34}S_{barite}$ values. Equation for open system Rayleigh fractionation from Canfield (2001b).

rates of AOM-SR increase with temperature, up to around 90 °C (Wankel et al., 2012). Therefore the discrepancy in bulk rock $\delta^{34}S$ composition between TYK-5 and 76-17 could represent greater advection of methane-rich diagenetic fluids in sediments proximal to the hydrothermal system. Subtle alteration has also been identified in mudstones located within 15 metres (above and below) of the bedded mineralisation, which preserve no visible evidence (i.e. veining, sulphide mineralisation) of hydrothermal input (Magnall et al., 2015). The correspondence between intensified AOM-SR with subtle alteration forms an interesting relationship, which demonstrates how the hydrothermal system may have perturbed background diagenetic processes within sediments proximal to hydrothermal activity. A greater contribution by Stage 2 pyrite to the bulk rock $\delta^{34}S$ values in samples from TYK-5 is consistent with the range of $\delta^{34}S_{barite}$ values produced in the open system model (Fig. 11). Notably, the coupling of bulk rock and micro-analytical data highlights the sensitivity of $\delta^{34}S_{sulphate}$ values to the combined effects of isotopic fractionation ($\varepsilon^{34}S$) and also the mass balance of different pathways of sulphate reduction.

5.4. Implications for SHMS mineralisation – Macmillan Pass and other deposits

In this study, we have documented two stages of diagenesis that precede hydrothermal mineralisation, all of which occurred beneath the SWI. Contrary to previous studies, the isotopic data do not support a model of quantitative sulphate reduction in a euxinic water column. This presents an interesting question, relating to the origin of reduced sulphur in these systems.

The hydrothermal pyrite (py-III) preserves a broad distribution of $\delta^{34}S$ values (~+3.0 to +18.6‰), which overlap with py-II, but also extend to lower values. This broad distribution of $\delta^{34}S_{pyrite}$ values is characteristic of sulphides forming in SHMS systems (Leach et al., 2005). Furthermore, the negative (py-I) and positive (py-II) end member $\delta^{34}S$ values are consistent with other studies that have acquired high resolution isotopic data from sulphides in SHMS deposits (e.g. Eldridge et al., 1988, 1993; Kelley et al., 2004b; Ireland et al., 2004) and also Irish-type deposits (Anderson et al., 1998; Barrie et al., 2009). Previously, this distribution of $\delta^{34}S$ values has been linked either with there being two different sources of sulphur (BSR and TSR) or with the development of closed system conditions (and associated Rayleigh-type effects) during the evolution of the deposit (e.g. Large et al., 2005). Importantly, the development of closed system conditions introduces mass balance limitations for sulphide formation; this is particularly relevant for periods of low seawater sulphate, which coincide with periods of SHMS formation during the Proterozoic and Paleozoic (Wilkinson, 2014). In this study we have demonstrated how positive $\delta^{34}S_{pyrite}$ values developed in open system conditions close to the SWI, which will have had important implications for maintaining the availability of sulphur (from seawater sulphate) to the host rock. Indeed, it is interesting that one of the largest SHMS deposits (Red Dog) is hosted in bioturbated mudstones (Reynolds et al., 2015), which would have enhanced porewater exchange with overlying seawater during diagenesis.

Finally, evidence of barite dissolution is commonplace in the bedded mineralisation at Tom and Jason (Fig. 6e), where it is associated with the formation of witherite, hydrothermal pyrite and sphalerite (Stage 3; Fig. 4). Therefore it is possible that the hydrothermal system also derived sulphur from barite dissolution, which would provide an additional mechanism for the generation of positive $\delta^{34}S$ values in py-III. Barite solubility switches from prograde to retrograde at 100 °C (Bowers et al., 1984), and increasing temperatures during the onset of hydrothermal activity would have produced a thermal regime favourable for barite dissolution. Barite replacement by sulphides has also been documented at Red Dog (Kelley et al., 2004a), and so may be an important pathway of sulphide formation in other SHMS systems enriched in barite (e.g. Rammelsberg; Large and Walcher, 1999). Ultimately, it is highly unlikely that any one single factor (e.g. euxinia) can be implicated as forming a metal trap for SHMS deposits in basins such as the Selwyn Basin, but rather it is a combination of factors that contribute to mineralisation. Certainly, we argue that it is more reasonable to concentrate sulphur in a host rock via multiple diagenetic pathways (barite precipitation, BSR, AOM-SR), than it is to achieve this exclusively in the water column.

6. CONCLUSIONS

A common feature of shale hosted massive sulphide (SHMS) deposits is the preservation of stratiform sulphides with positive $\delta^{34}S$ values. In the conventional model for Selwyn Basin SHMS deposits (*Selwyn Basin model*), stratiform mineralisation forms following water column precipitation of barite, pyrite and Zn–Pb sulphides (sphalerite, galena). The source of reduced sulphur in the Selwyn Basin model, and the isotopic characteristics of barite and sulphides, is controlled by the near quantitative reduction of seawater sulphate and the development of euxinic conditions. In this study, we have identified multiple generations of barite (brt-I, II, III) and pyrite (py-I, IIa, IIb ± III) in both stratiform mineralisation (Tom, Jason deposits) and un-mineralised mudstones from Late Devonian Selwyn Basin strata (Macmillan Pass, YT). It is therefore clear that the use of isotopic data obtained via micro-analytical techniques such as SIMS (*secondary ion mass spectrometry*; SIMS) is required, in tandem with bulk techniques, to fully assess the cycling of sulphur in these types of systems.

In contrast to the *Selwyn Basin model*, the petrographic and isotopic data produced from stratiform features in mineralised samples from Macmillan Pass are more consistent with diagenetic processes (i.e. formation beneath the sediment water interface; SWI). The $\delta^{34}S$ values of three generations of barite overlap (+22.5 to +33.0 ‰) and preserve no evidence to suggest the sulphate source (i.e. seawater) underwent near quantitative sulphate reduction. Furthermore, barite pre-dates all evidence of hydrothermal input (Zn-Pb-Fe sulphides). Together, this rules out a hydrothermal origin for barite, and precipitation from a restricted, euxinic water column. This conclusion raises an interesting problem, concerning what forms the metal 'trap' for base metals in such mineralised systems.

We find that there is widespread textural and mineralogical evidence of barite replacement by hydrothermal sulphides. Furthermore, in the isotopic relationship between barite (brt-II) and pyrite (py-IIa), where $\delta^{34}S_{pyrite} \approx \delta^{34}S_{barite}$, there is evidence of sulphate reduction coupled with anoxic oxidation of methane (AOM-SR). This process was highly effective at reducing pore water sulphate (to H_2S), locally, in nearly quantitative proportions, thereby producing positive $\delta^{34}S_{pyrite}$ values. Bulk rock $\delta^{34}S_{pyrite}$ values, obtained from un-mineralised mudstone samples from two drill holes (TYK-5 and 76-17), suggest this process may have been intensified by hydrothermal convection of diagenetic fluids. Notably, the magnitude of the isotopic fractionation associated with sulphate reduction during Stage 2 ($\varepsilon^{34}S < 15‰$) is markedly reduced relative to Stage 1 ($\varepsilon^{34}S \leq 60‰$). Therefore, the distribution of coeval $\delta^{34}S_{sulphate}$ values (as recorded by $\delta^{34}S_{barite}$) were sensitive to the relative contribution of reduced sulphur generated during Stages 1 and 2, and can be explained by an open system Rayleigh fractionation model. Together, we argue that pre-existing barite enrichments and AOM-SR would have

proven highly effective in concentrating sulphur beneath the SWI at Macmillan Pass. Ultimately, the interplay between biological activity, methanogenesis (and AOM-SR), seawater sulphate concentrations, and open system diagenesis represent important parameters to consider when interpreting $\delta^{34}S$ values in SHMS and barite deposits from the geologic record.

ACKNOWLEDGEMENTS

We acknowledge the careful and insightful reviews of Craig Johnson and an anonymous reviewer and also the helpful comments from associate editor Ed Ripley. We would like to thank the Geological Survey of Canada, and specifically the TGI-4 initiative for funding the project, along with an NSERC Discovery Grant to SG. Hudbay Mineral Resources are thanked for allowing access to the drill-core and camp at Macmillan Pass. ESS Contribution number / Numéro de contribution du SST: 20150422.

APPENDIX A. SUPPLEMENTARY DATA

Supplementary data associated with this article can be found, in the online version, at http://dx.doi.org/10.1016/j.gca.2016.02.015.

REFERENCES

Aharon P. and Fu B. (2000) Microbial sulfate reduction rates and sulfur and oxygen isotope fractionations at oil and gas seeps in deepwater Gulf of Mexico. *Geochim. Cosmochim. Acta* **64**, 233–246.

Aller R. C. (2014) Sedimentary diagenesis, depositional environments, and benthic fluxes. In *Treatise on Geochemistry* (eds. H. D. Holland and K. K. Turekian). Elsevier Ltd., pp. 293–334.

Aller R. C., Madrid V., Chistoserdov A., Aller J. Y. and Heilbrun C. (2010) Unsteady diagenetic processes and sulfur biogeochemistry in tropical deltaic muds: Implications for oceanic isotope cycles and the sedimentary record. *Geochim. Cosmochim. Acta* **74**, 4671–4692.

Anderson I. K., Ashton J. H., Boyce A. J., Fallick A. E. and Russel M. J. (1998) Ore depositional processes in the Navan Zn–Pb deposit, Ireland. *Econ. Geol.*.

Ansdell K. M., Nesbitt B. E. and Longstaffe F. J. (1989) A fluid inclusion and stable isotope study of the Tom Ba–Pb–Zn deposit, Yukon Territory, Canada. *Econ. Geol.* **84**, 841–856.

Antler G., Turchyn A. V., Rennie V., Herut B. and Sivan O. (2013) Coupled sulfur and oxygen isotope insight into bacterial sulfate reduction in the natural environment. *Geochim. Cosmochim. Acta* **118**, 98–117.

Arndt S., Hetzel A. and Brumsack H.-J. (2009) Evolution of organic matter degradation in Cretaceous black shales inferred from authigenic barite: A reaction-transport model. *Geochim. Cosmochim. Acta* **73**, 2000–2022.

Arning E. T., Gaucher E. C., van Berk W. and Schulz H.-M. (2015) Hydrogeochemical models locating sulfate-methane transition zone in marine sediments overlying black shales: a new tool to locate biogenic methane? *Mar. Pet. Geol.* **59**, 563–574.

Bailes R. J., Smee B. W., Blackader D. W. and Gardner H. D. (1986) Geology of the Jason lead-zinc-silver deposits, Macmillan Pass, Eastern Yukon. In *Mineral Deposits of Northern Cordillera* (ed. J. A. Morin). The Canadian Institute of Mining and Metallurgy, pp. 87–99.

Barnes R. O. and Goldberg E. D. (1976) Methane production and consumption in anoxic marine sediments. *Geology* **4**, 297–300.

Barrie C. D., Boyce A. J., Boyle A. P., Williams P. J., Blake K., Wilkinson J. J., Lowther M., Mcdermott P. and Prior D. J. (2009) On the growth of colloform textures: a case study of sphalerite from the Galmoy ore body. *Ireland. J. Geol. Soc. London* **166**, 563–582.

Berner R. A. (1980) Early Diagenesis: A Theoretical Approach. Princeton University Press.

Bishop J. K. B. (1988) The barite-opal-organic carbon association in oceanic particulate matter. *Nature* **332**, 341–343.

Borowski W. S., Rodriguez N. M., Paull C. K. and Ussler W. (2013) Are 34S-enriched authigenic sulfide minerals a proxy for elevated methane flux and gas hydrates in the geologic record? *Mar. Pet. Geol.* **43**, 381–395.

Bottrell S. H. and Newton R. J. (2006) Reconstruction of changes in global sulfur cycling from marine sulfate isotopes. *Earth Sci. Rev.* **75**, 59–83.

Bowers T. S., Jackson K. J. and Helgeson H. C. (1984) Equilibrium activity diagrams. Springer-Verlag, Berlin.

Bradley A. S., Leavitt W. D. and Johnston D. T. (2011) Revisiting the dissimilatory sulfate reduction pathway. *Geobiology* **9**, 446–457.

Brunner B. and Bernasconi S. M. (2005) A revised isotope fractionation model for dissimilatory sulfate reduction in sulfate reducing bacteria. *Geochim. Cosmochim. Acta* **69**, 4759–4771.

Canfield D. E. (2001a) Biogeochemistry of Sulfur Isotopes. *Rev. Mineral. Geochemistry* **43**, 607–636.

Canfield D. E. (2001b) Isotope fractionation by natural populations of sulfate-reducing bacteria. *Geochim. Cosmochim. Acta* **65**, 1117–1124.

Canfield D. E. (2004) The evolution of the earth surface sulfur reservoir. *Am. J. Sci.* **304**, 839–861.

Canfield D. E. and Thamdrup B. (1994) The production of ^{34}S-depleted sulfide during bacterial disproportionation of elemental sulfur. *Science (80-.)* **266**, 1973–1975.

Canfield D. E., Raiswell R., Westrich J. T., Reaves C. M. and Berner R. A. (1986) The use of chromium reduction in the analysis of reduced inorganic sulfur in sediments and shales. *Chem. Geol.* **54**, 149–155.

Carne R. C. and Cathro R. J. (1982) Sedimentary exhalative (sedex) zinc-lead-silver deposits, northern Canadian Cordillera. *Can. Min. Metall. Bull.* **75**, 66–78.

Cecile M. P., Shakur M. A. and Krouse H. R. (1983) The isotopic composition of western Canadian barites and the possible derivation of oceanic sulphate δ34S and δ18O age curves. *Can. J. Earth Sci.* **20**, 1528–1535.

Chen D., Wang J., Racki G., Li H., Wang C., Ma X. and Whalen M. T. (2013) Large sulphur isotopic perturbations and oceanic changes during the Frasnian–Famennian transition of the Late Devonian. *J. Geol. Soc. London* **170**, 465–476.

Cruse A. M. and Seewald J. S. (2006) Geochemistry of low-molecular weight hydrocarbons in hydrothermal fluids from Middle Valley, northern Juan de Fuca Ridge. *Geochim. Cosmochim. Acta* **70**, 2073–2092.

Dawson K. M. and Orchard M. J. (1982) Regional metallogeny of the northern Cordillera: biostratigraphy, correlation and metallogenic significance of bedded barite occurrences in eastern Yukon and western District of Mackenzie. *Geol. Surv. Canada*, 31–38, Pap. 82-1C.

Dehairs F., Chesselet R. and Jedwab J. (1980) Discrete suspended particles of barite and the barium cycle in the open ocean. *Earth Planet. Sci. Lett.* **49**, 528–550.

Deusner C., Holler T., Arnold G. L., Bernasconi S. M., Formolo M. J. and Brunner B. (2014) Sulfur and oxygen isotope

fractionation during sulfate reduction coupled to anaerobic oxidation of methane is dependent on methane concentration. *Earth Planet. Sci. Lett.* **399**, 61–73.

Dickens G. R. D. (2001) Sulfate profiles and barium fronts in sediment on the Blake Ridge : Present and past methane fluxes through a large gas hydrate reservoir. *Geochim. Cosmochim. Acta* **65**, 529–543.

Dymond J. and Collier R. (1996) Particulate barium fluxes and their relationships to biological productivity. *Deep Sea Res. Part II* **43**, 1283–1308.

Eldridge C. S., Compston W., Williams I. S., Both R. A., Walshe J. L. and Ohmoto H. (1988) Sulfur isotope variability in sediment-hosted massive sulfide deposits as determined using the ion microprobe SHRIMP: 1. An example from the Rammelsberg orebody. *Econ. Geol.* **83**, 443–449.

Eldridge C. S., Williams N. and Walshe J. L. (1993) Sulfur isotope variability in sediment-hosted massive sulfide deposits as determined using the ion microprobe SHRIMP: II. A study of the H.Y.C. deposit at McArthur River, Northern Territory, Australia. *Econ. Geol.* **88**, 1–26.

Emerson, S. and Hedges, J. (eds.) (2003) *Sediment diagenesis and benthic flux*Holland, H. D. and Turekian, K. K. (eds.) (2003) Treatise on Geochemistry.

Farquhar J., Nanping W., Canfield D. E. and Oduro H. (2010) Connections between Sulfur Cycle Evolution, Sulfur Isotopes, Sediments, and Base Metal Sulfide Deposits. *Econ. Geol.* **105**, 509–533.

Fike D. A., Bradley A. S. and Rose C. V. (2015) Rethinking the ancient sulfur cycle. *Annu. Rev. Earth Planet. Sci.* **43**, 593–622.

Fritz P., Basharmal G. M., Drimmie R. J., Ibsen J. and Qureshi R. M. (1989) Oxygen isotope exchange between sulphate and water during bacterial reduction of sulphate. *Chem. Geol. Isot. Geosci. Sect.* **79**, 99–105.

Froelich P. N., Klinkhammer G. P., Bender M. L., Luedtke N. A., Heath G. R., Cullen D., Dauphin P., Hammond D. and Hartman B. (1979) Early oxidation of organic matter in pelagic sediments of the eastern equatorial Atlantic: suhoxic diagenesis. *Geochim. Cosmochim. Acta.*.

Gadd M. G., Layton-Matthews D., Peter J. M. and Paradis S. J. (2015) The world-class Howard's Pass SEDEX Zn-Pb district, Selwyn Basin, Yukon. Part I: trace element compositions of pyrite record input of hydrothermal, diagenetic, and metamorphic fluids to mineralization. *Miner. Depos.*, 1–24.

Gardner H. D. and Hutcheon I. (1985) Geochemistry, Mineralogy, and Geology of the Jason Pb-Zn Deposits, Macmillan Pass, Yukon. *Canada. Econ. Geol.* **80**, 1257–1276.

Goldhaber M. B. and Kaplan I. R. (1975) Controls and consequences of sulfate reduction rates in recent marine sediments. *Soil Sci.* **119**, 42–55.

Gomes M. L. and Hurtgen M. T. (2015) Sulfur isotope fractionation in modern euxinic systems: Implications for paleoenvironmental reconstructions of paired sulfate–sulfide isotope records. *Geochim. Cosmochim. Acta* **157**, 39–55.

Gonzalez-Munoz M. T., Martinez-Ruiz F., Morcillo F., Martin-Ramos J. D., Paytan A., Gonzalez-Muñoz M. T., Martinez-Ruiz F., Morcillo F., Martin-Ramos J. D. and Paytan A. (2012) Precipitation of barite by marine bacteria: A possible mechanism for marine barite formation. *Geology* **40**, 675–678.

Goodfellow W. D. (1987) Anoxic stratified oceans as a source of sulphur in sediment-hosted stratiform Zn–Pb Deposits (Selwyn Basin, Yukon, Canada). *Chem. Geol. (Isotope Geosci. Sect.)* **65**, 359–382.

Goodfellow W. D. (2007) Base metal metallogeny of the Selwyn Basin, Canada. In *Mineral Deposits of Canada: A Synthesis of Major Deposit-Types, District Metallogeny, the Evolution of Geological Provinces, and Exploration Methods* (ed. W. D. Goodfellow). Geological Association of Canada, pp. 553–579.

Goodfellow W. D. and Jonasson I. R. (1984) Ocean stagnation and ventilation defined by 34-S secular trends in pyrite and barite, Selwyn Basin, Yukon. *Geology* **12**, 583–586.

Goodfellow W. D. and Jonasson I. R. (1986) Environment of formation of the Howards Pass (XY) Zn-Pb deposit, Selwyn Basin, Yukon. In *Mineral Deposits of Northern Cordillera* (ed. J. A. Morin). The Canadian Institute of Mining and Metallurgy, pp. 19–50.

Goodfellow W. D. and Lydon J. W. (2007) Sedimentary exhalative (SEDEX) deposits. In *Mineral Deposits of Canada: A Synthesis of Major Deposit-Types, District Metallogeny, the Evolution of Geological Provinces, and Exploration Methods* (ed. W. D. Goodfellow). Geological Association of Canada, pp. 163–183.

Gordey S. P. and Anderson R. G. (1993) Evolution of the northern cordilleran miogeocline, Nahanni map area (105I), Yukon and Northwest Territories. In *Memoir 428* (eds. S. P. Gordey and R. G. Anderson). Geological Survey of Canada.

Habicht K. S. and Canfield D. E. (1997) Sulfur isotope fractionation during bacterial sulfate reduction in organic-rich sediments. *Geochim. Cosmochim. Acta* **61**, 5351–5361.

Habicht K. S., Gade M., Thamdrup B., Berg P. and Canfield D. E. (2002) Calibration of sulfate levels in the Archean ocean. *Science (80-.)* **298**, 2372–2374.

Harrison A. G. G. and Thode H. G. (1958) Mechanism of the bacterial reduction of sulphate from isotope fractionation studies. *Trans. Faraday Soc.* **54**, 84–92.

Henkel S., Mogollón J. M., Nöthen K., Franke C., Bogus K., Robin E., Bahr A., Blumenberg M., Pape T., Seifert R., März C., de Lange G. J. and Kasten S. (2012) Diagenetic barium cycling in Black Sea sediments – A case study for anoxic marine environments. *Geochim. Cosmochim. Acta* **88**, 88–105.

Hoehler T. M., Alperin M. J., Albert D. B. and Martens C. S. (1994) Field and laboratory studies of methane oxidation in an anoxic marine sediment: Evidence for a methanogen-sulfate reducer consortium. *Global Biogeochem. Cycles* **8**, 451.

Horita J., Zimmerman H. and Holland H. D. (2002) Chemical evolution of seawater during the Phanerozoic : Implications from the record of marine evaporites. *Geochim. Cosmochim. Acta* **66**, 3733–3756.

Ireland T., Large R. R., McGoldrick P. and Blake M. (2004) Spatial distribution patterns of sulfur isotopes, nodular carbonate, and ore textures in the McArthur River (HYC) Zn–Pb–Ag deposit, Northern Territory, Australia. *Econ. Geol.* **99**, 1687–1709.

Irwin S. and Orchard M. (1989) Conodont biostratigraphy and constraints on Upper Devonian mineral deposits in the Earn Group, northern British Columbia and Yukon. *Current Research, Part E*. Geological Survey of Canada, pp. 13–19, Paper 89–1E.

Irwin S. E. B. and Orchard M. J. (1991) Upper Devonian–Lower Carboniferous conodont biostratigraphy of the Earn Group and overlying units, northern Cordillera. In *Ordovician to Triassic Conodont Paleontology of the Canadian Cordillera* (eds. M. J. Orchard and A. D. McCracken). Geological Survey of Canada, Bulletin 417. pp. 185–213.

Iversen N. and Jørgensen B. B. (1985) Anaerobic methane oxidation rates at the sulfate-methane transition in marine sediments from Kattegat and Skagerrak (Denmark). *Limnol. Oceanogr.* **1985**, 944–955.

John E. H., Wignall P. B., Newton R. J. and Bottrell S. H. (2010) Δ34SCAS and δ18OCAS records during the Frasnian–Famennian (Late Devonian) transition and their bearing on mass extinction models. *Chem. Geol.* **275**, 221–234.

Johnson C. A., Kelley K. D. and Leach D. L. (2004) Sulfur and Oxygen Isotopes in Barite Deposits of the Western Brooks Range, Alaska, and Implications for the Origin of the Red Dog Massive Sulfide Deposits. *Econ. Geol.* **99**, 1435–1448.

Johnson C. A., Emsbo P., Poole F. G. and Rye R. O. (2009) Sulfur- and oxygen-isotopes in sediment-hosted stratiform barite deposits. *Geochim. Cosmochim. Acta* **73**, 133–147.

Jones D. S. and Fike D. A. (2013) Dynamic sulfur and carbon cycling through the end-Ordovician extinction revealed by paired sulfate–pyrite δ34S. *Earth Planet. Sci. Lett.* **363**, 144–155.

Jørgensen B. B. J. and Kasten S. (2006) Sulfur Cycling and Methane Oxidation. In *Marine Geochemistry* (eds. H. D. Schulz and M. Zabel). Springer, Berlin Heidelberg, pp. 271–309.

Jørgensen B. B., Böttcher M. E., Lüschen H., Neretin L. N. and Volkov I. I. (2004) Anaerobic methane oxidation and a deep H2S sink generate isotopically heavy sulfides in Black Sea sediments. *Geochim. Cosmochim. Acta* **68**, 2095–2118.

Joye S. B., Boetius A., Orcutt B. N., Montoya J. P., Schulz H. N., Erickson M. J. and Lugo S. K. (2004) The anaerobic oxidation of methane and sulfate reduction in sediments from Gulf of Mexico cold seeps. *Chem. Geol.* **205**, 219–238.

Kaplan I. R. and Rittenberg S. C. (1964) Microbiological Fractionation of Sulphur Isotopes. *J. Gen. Microbiol.* **34**, 195–212.

Kasten S., Freudenthal T., Gingele F. X. and Schulz H. D. (1998) Simultaneous formation of iron-rich layers at different redox boundaries in sediments of the Amazon deep-sea fan. *Geochim. Cosmochim. Acta* **62**, 2253–2264.

Kelley K. D., Dumoulin J. A. and Jennings S. (2004a) The Anarraaq Zn–Pb–Ag and barite deposit, Northern Alaska: evidence for replacement of carbonate by barite and sulfides. *Econ. Geol.* **99**, 1577–1591.

Kelley K. D., Leach D. L., Johnson C. A., Clark J. L., Fayek M., Slack J. F., Anderson V. M., Ayuso R. A. and Ridley W. I. (2004b) Textural, Compositional, and Sulfur Isotope Variations of Sulfide Minerals in the Red Dog Zn-Pb-Ag Deposits, Brooks Range, Alaska: Implications for Ore Formation. *Econ. Geol.* **99**, 1509–1532.

Kiyosu Y. and Krouse R. H. (1990) The role of organic and acid the in the sulfur abiogenic isotope reduction effect. *Geochem. J.* **24**, 21–27.

Knittel K. and Boetius A. (2009) Anaerobic Oxidation of Methane: Progress with an Unknown Process. *Annu. Rev. Microbiol.* **63**, 311–334.

Kozdon R., Kita N. T., Huberty J. M., Fournelle J. H., Johnson C. A. and Valley J. W. (2010) In situ sulfur isotope analysis of sulfide minerals by SIMS: precision and accuracy, with application to thermometry of ~3.5 Ga Pilbara cherts. *Chem. Geol.* **275**, 243–253.

Large D. and Walcher E. (1999) The Rammelsberg massive sulphide Cu-Zn-Pb-Ba-Deposit, Germany: An example of sediment-hosted, massive sulphide mineralisation. *Miner. Depos.* **34**, 522–538.

Large R. R., Bull S. W., McGoldrick P. J., Walters S., Derrick G. M. and Carr G. R. (2005) Strata-Bound and stratiform Zn-Pb-Ag deposits in proterozoic sedimentary basins, Northern Australia. *Econ. Geol.* **100**, 931–963.

Leach D. L., Sangster D. F., Kelley K. D., Large R. R., Garven G., Allen C. R., Gutzmer J. and Walters J. (2005) Sediment-hosted lead-zinc deposits a global perspective. In *Economic Geology 100th Anniversary Volume* (eds. J. W. Hedenquist, J. F. H. Thompson, R. J. Goldfarb and J. P. Richards). Economic Geology Publishing Co., pp. 561–607.

Leach D. L., Bradley D. C., Huston D., Pisarevsky S. A., Taylor R. D. and Gardoll J. (2010) Sediment-Hosted Lead-Zinc Deposits in Earth History. *Econ. Geol.* **105**, 593–625.

Lyons T. W. (1997) Sulfur isotopic trends and pathways of iron sulfide formation in upper Holocene sediments of the anoxic Black Sea. *Geochim. Cosmochim. Acta* **61**, 3367–3382.

Lyons T. W., Gellatly A. M., Mcgoldrick P. J. and Kah L. C. (2006) Proterozoic sedimentary exhalative (SEDEX) deposits and links to evolving ocean chemistry. *Geol. Soc. Am. Mem.* **198**, 169–184.

Machel H. G. (2001) Bacterial and thermochemical sulfate reduction in diagenetic settings - old and new insights. *Sediment. Geol.* **140**, 143–175.

Machel H. G., Krouse H. R. and Sassen R. (1995) Products and distinguishing criteria of bacterial and thermochemical sulfate reduction. *Appl. Geochemistry* **10**, 373–389.

Magnall J. M., Gleeson S. A. and Paradis S. (2015) The importance of siliceous radiolarian-bearing mudstones in the formation of sediment-hosted Zn-Pb±Ba mineralization in the Selwyn Basin, Yukon. *Canada. Econ. Geol.* **110**, 2139–2146.

McClay K. R. (1991) Deformation of stratiform Zn-Pb (-barite) deposits in the northern Canadian Cordillera. *Ore Geol. Rev.* **6**, 435–462.

McClay K. R. and Bidwell G. E. (1986) Geology of the Tom deposit, Macmillan Pass, Yukon. In *Mineral Deposits of Northern Cordillera* (ed. J. A. Morin). The Canadian Institute of Mining and Metallurgy, pp. 100–114.

Mizutani Y. and Rafter T. A. (1973) Isotopic behavior of sulphate oxygen in the bacterial reduction of sulphate. *Geochem. J.* **6**, 183–191.

Morganti J. M. (1979) The geology and ore deposits of the Howards Pass area, Yukon and Northwest Territories: the origin of basinal sedimentary stratiform sulphide deposits. University of British Columbia.

Nelson J. L., Colpron M., Piercey S. J., Dusel-Bacon C., Murphy D. C. and Roots C. F. (2006) Paleozoic tectonic and metallogenetic evolution of pericratonic terranes in Yukon, northern British Columbia and eastern Alaska. In *Paleozoic Evolution and Metallogeny of Pericratonic Terranes at the Ancient Pacific Margin of North America, Canadian and Alaskan Cordillera* (eds. M. Colpron and J. L. Nelson). pp. 323–360.

Neretin L. N., Böttcher M. E., Jørgensen B. B., Volkov I. I., Lüschen H. and Hilgenfeldt K. (2004) Pyritization processes and greigite formation in the advancing sulfidization front in the Upper Pleistocene sediments of the Black Sea. *Geochim. Cosmochim. Acta* **68**, 2081–2093.

Newton R. J., Reeves E. P., Kafousia N., Wignall P. B., Bottrell S. H. and Sha J.-G. (2011) Low marine sulfate concentrations and the isolation of the European epicontinental sea during the Early Jurassic. *Geology* **39**, 7–10.

Niewöhner C., Hensen C., Kasten S., Zabel M. and Schulz H. D. (1998) Deep sulfate reduction completely mediated by anaerobic methane oxidation in sediments of the upwelling area off Namibia. *Geochim. Cosmochim. Acta*.

Ohmoto H. and Goldhaber M. B. (1997) Sulfur and carbon isotopes. In *Geochemistry of Hydrothermal Ore Deposits* (ed. H. L. Barnes). John Wiley & Sons, pp. 517–612.

Passier H. F., Middelburg J. J., De Lange G. J. and Böttcher M. E. (1997) Pyrite contents, microtextures, and sulfur isotopes in relation to formation of the youngest eastern Mediterranean sapropel. *Geology* **25**, 519–522.

Paytan A. and Griffith E. M. (2007) Marine barite: Recorder of variations in ocean export productivity. *Deep Sea Res. Part II* **54**, 687–705.

Paytan A., Mearon S., Cobb K. and Kastner M. (2002) Origin of marine barite deposits: Sr and S isotope characterization. *Geology* **30**, 747.

Pigage L. C. (1991) Field guide Anvil Pb–Zn–Ag District, Yukon Territory, Canada. In: *Geological Survey of Canada Open File* 2169 (eds. J. G. Abbott and R. J. W. Turner). pp. 177–244.

Raiswell R. (1982) Pyrite texture, isotopic composition and the availability of iron. *Am. J. Sci.* **282**, 1244–1263.

Reeburgh W. S. (1976) Methane consumption in cariaco trench waters and sediments. *Earth Planet. Sci. Lett.* **28**, 337–344.

Rees C. E. (1973) A steady-state model for sulphur isotope fractionation in bacterial reduction processes. *Geochim. Cosmochim. Acta* **37**, 1141–1162.

Reynolds M. A., Gingras M. K., Gleeson S. A. and Stemler J. U. (2015) More than a trace of oxygen: Ichnological constraints on the formation of the giant Zn-Pb-Ag ± Ba deposits, Red Dog district, Alaska. *Geology* **43**, 867–870.

Schmitz B. (1987) Barium, equatorial high productivity, and the northward wandering of the Indian continent. *Paleoceanography* **2**, 63–77.

Stamatakis M. G. and Hein J. R. (1993) Origin of barite in Tertiary marine sedimentary rocks from Lefkas Island. *Greece. Econ. Geol.* **88**, 91–103.

Torres M. E., Brumsack H. J., Bohrmann G. and Emeis K. C. (1996) Barite fronts in continental margin sediments: a new look at barium remobilization in the zone of sulfate reduction and formation of heavy barites in diagenetic fronts. *Chem. Geol.* **127**, 125–139.

Torres M. E., Bohrmann G., Dubé T. E., Poole F. G., Poole Forrest G. and Poole F. G. (2003) Formation of modern and Paleozoic stratiform barite at cold methane seeps on continental margins. *Geology* **31**, 897–900.

Turner R. J. (1991) Jason stratiform Zn-Pb-barite deposit, Selwyn Basin, Canada (NTS 105-0-1): geological setting, hydrothermal facies and genesis (eds. J. G. Abbott and R. J. Turner). Geological Survey of Canada Open File 2169, pp. 137–175.

Turner R. J. W. (1992) Formation of Phanerozoic stratiform sediment, hosted zinc- lead deposits : Evidence for the critical role of ocean anoxia. *Chem. Geol.* **99**, 165–188.

Wankel S. D., Adams M. M., Johnston D. T., Hansel C. M., Joye S. B. and Girguis P. R. (2012) Anaerobic methane oxidation in metalliferous hydrothermal sediments: influence on carbon flux and decoupling from sulfate reduction. *Environ. Microbiol.* **14**, 2726–2740.

Wankel S. D., Bradley A. S., Eldridge D. L. and Johnston D. T. (2014) Determination and application of the equilibrium oxygen isotope effect between water and sulfite. *Geochim. Cosmochim. Acta* **125**, 694–711.

Widerlund A., Nowell G. M., Davison W. and Pearson D. G. (2012) High-resolution measurements of sulphur isotope variations in sediment pore-waters by laser ablation multicollector inductively coupled plasma mass spectrometry. *Chem. Geol.* **291**, 278–285.

Wilkin R. T., Barnes H. L. and Brantley S. L. (1996) The size distribution of framboidal pyrite in modern sediments: An indicator of redox conditions. *Geochim. Cosmochim. Acta* **60**, 3897–3912.

Wilkinson J. J. (2014) *Sediment-Hosted Zinc-Lead Mineralization: Processes and Perspectives*. Second Edition Elsevier Ltd., In Treatise on Geochemistry, pp. 219–249.

Wortmann U. G., Chernyavsky B., Bernasconi S. M., Brunner B., Böttcher M. E. and Swart P. K. (2007) Oxygen isotope biogeochemistry of pore water sulfate in the deep biosphere: Dominance of isotope exchange reactions with ambient water during microbial sulfate reduction (ODP Site 1130). *Geochim. Cosmochim. Acta* **71**, 4221–4232.

Associate editor: Edward M. Ripley